Tau Lepton Reconstruction and Identification in ATLAS

TAU2021, Indiana University
September 29, 2021

Christian Grefe

on behalf of the ATLAS collaboration

GEFÖRDERT VOM
Bundesministerium für Bildung und Forschung
ErUM-FSP T02 ATLAS

UNIVERSITÄT BONN

The ATLAS Detector

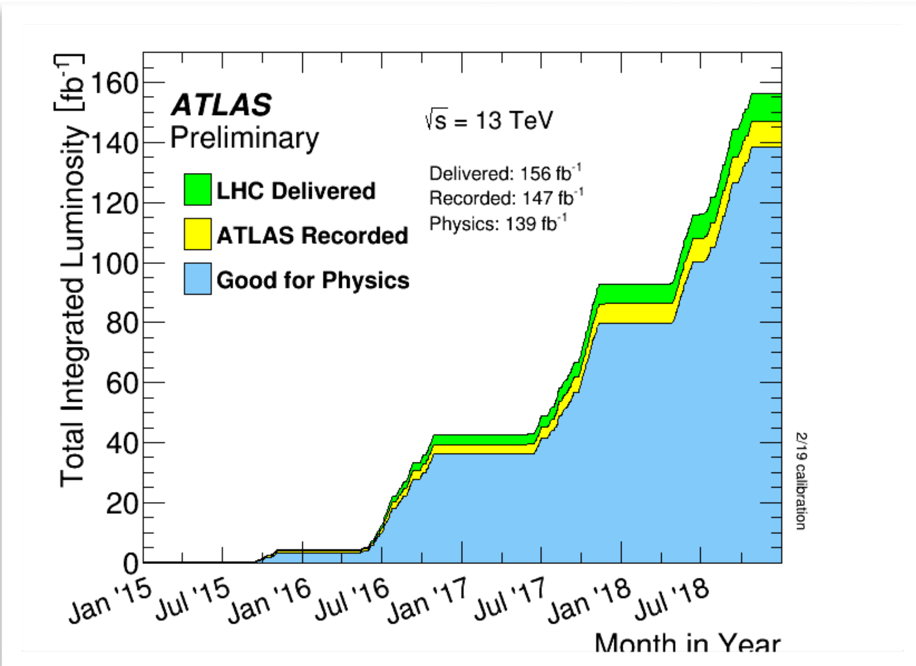

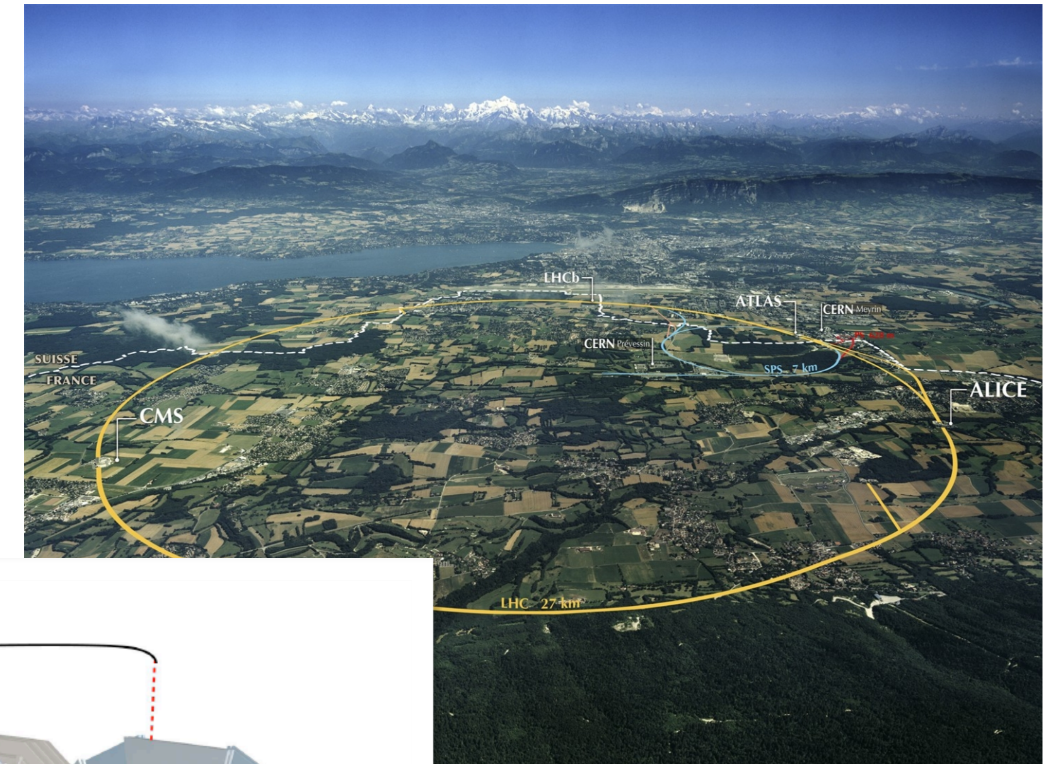

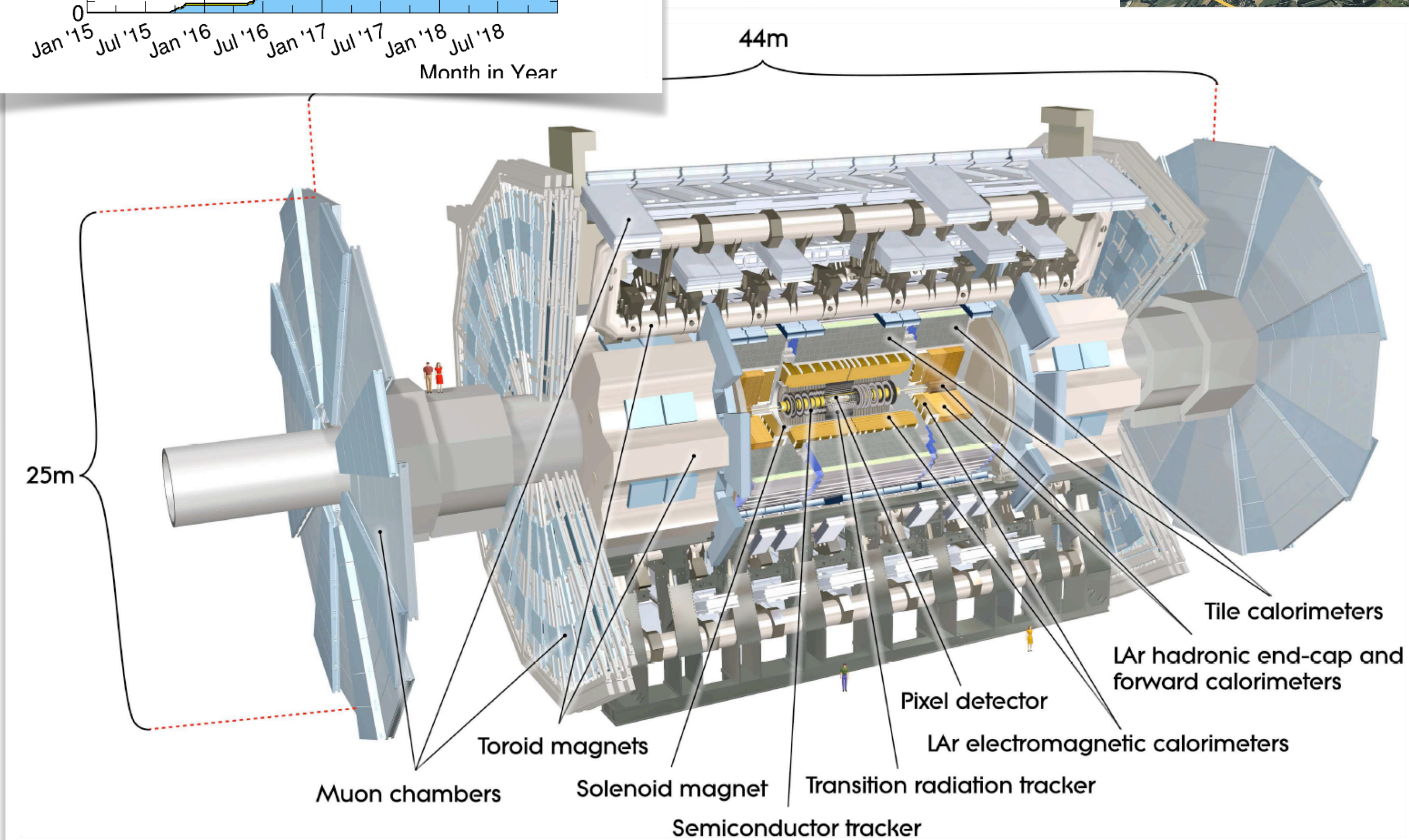

Reconstruction of τ-lepton decays

- Leptonic τ-lepton decays are reconstructed as electrons and muons (with possibly relaxed d_0 cuts at analysis level)

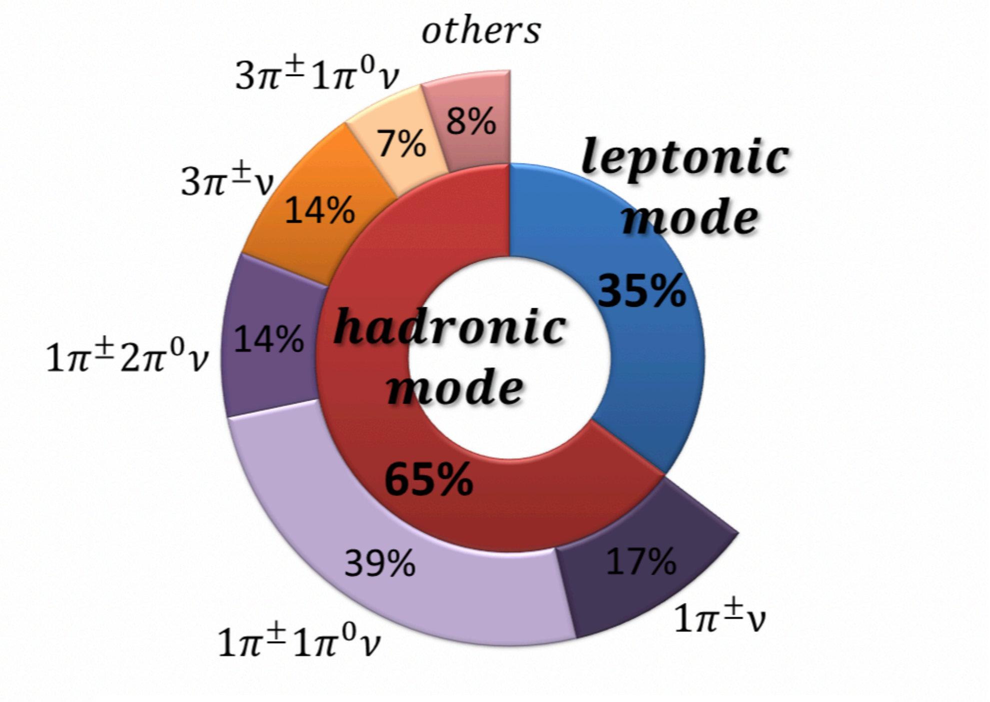

- Reconstruction of hadronic τ-lepton decays starts from anti-k_T jets with R=0.4 as seeds

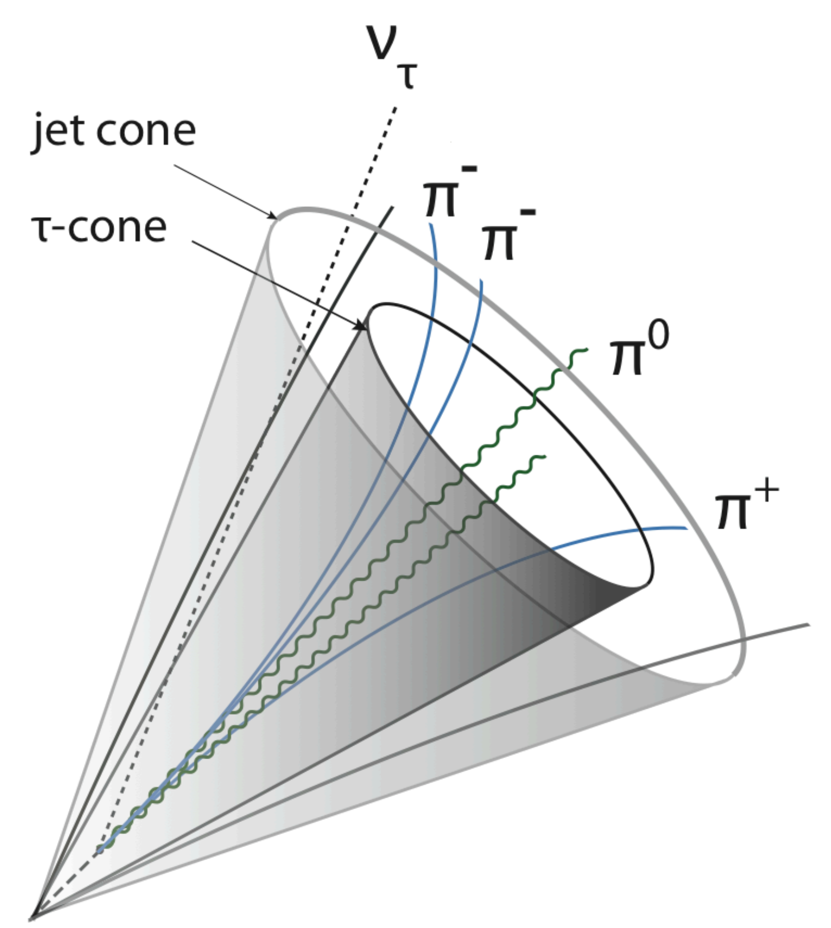

- Classify tracks within cone into tau, isolation, pile-up and conversion tracks using multiple BDTs - require exactly 1 or 3 tau-tracks

π^0 identification

- Subtract hadronic energy associated to tracks and use remaining energy to identify neutral particles (particle flow)
- Dedicated BDT (Tau Particle Flow) using EM cluster variables is used to identify π^0 clusters

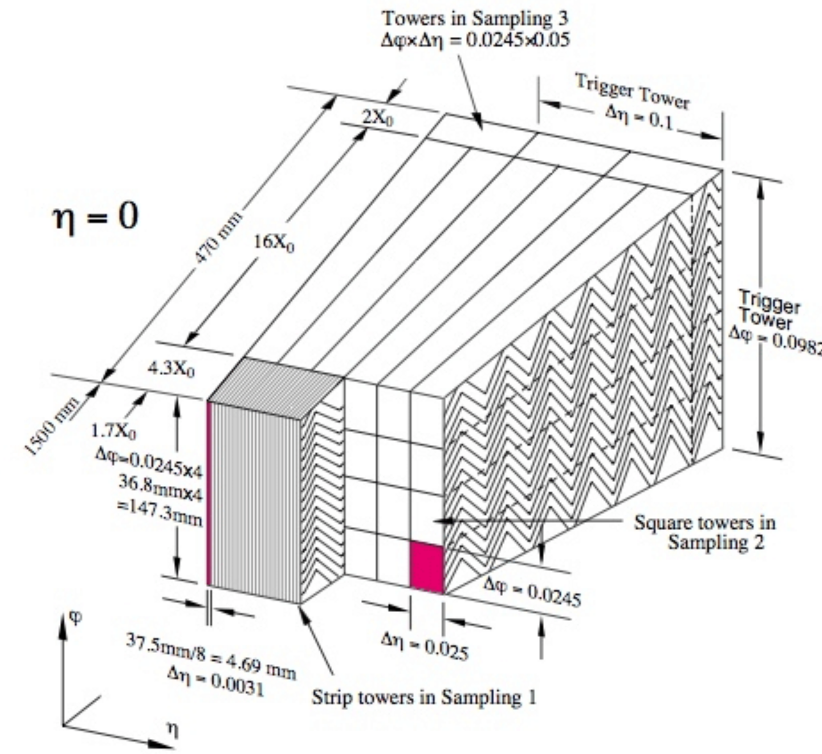

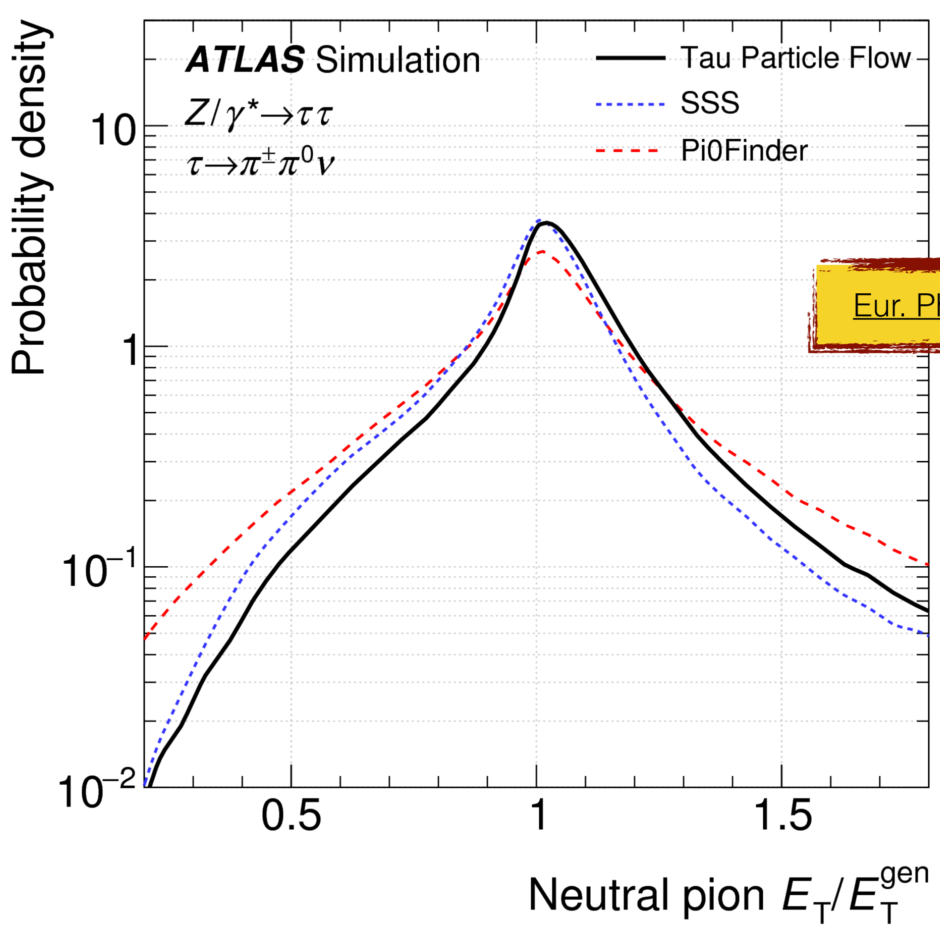

Eur. Phys. J C 76 (2016) 295

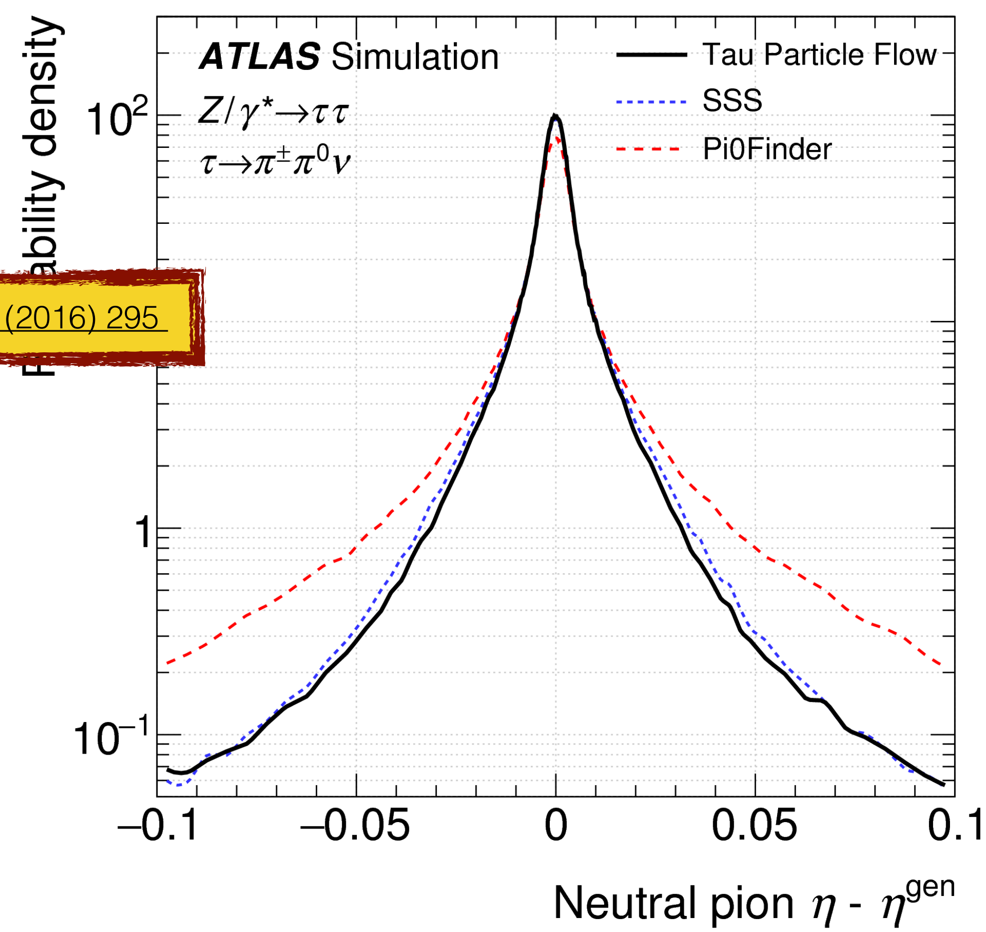

Decay Mode Classification

- 3 additional BDTs are used to identify five different decay modes using the output of the π^0 BDT and other observables

- Allows decay-mode specific fake tau estimates, construction of spin observables, etc.

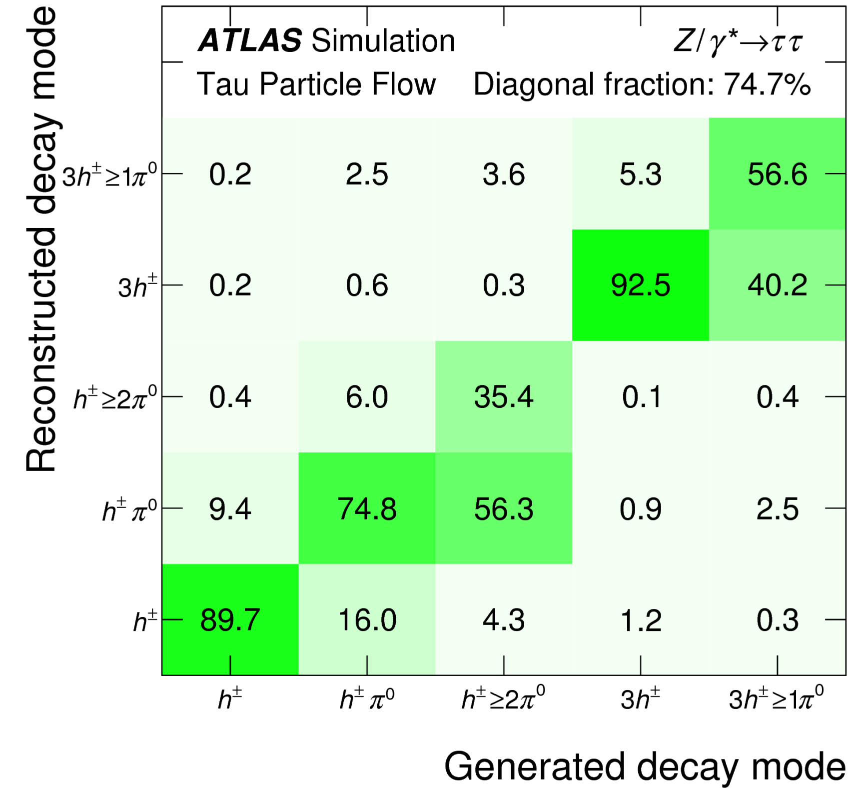

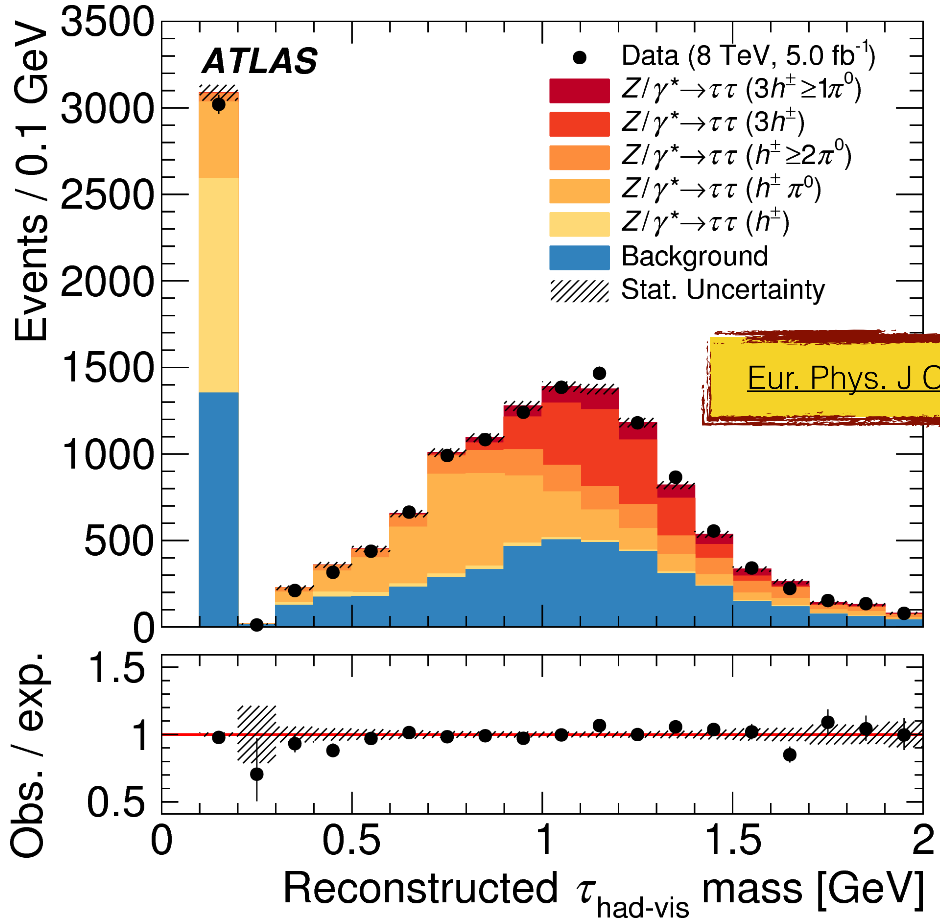

Eur. Phys. J C 76 (2016) 295

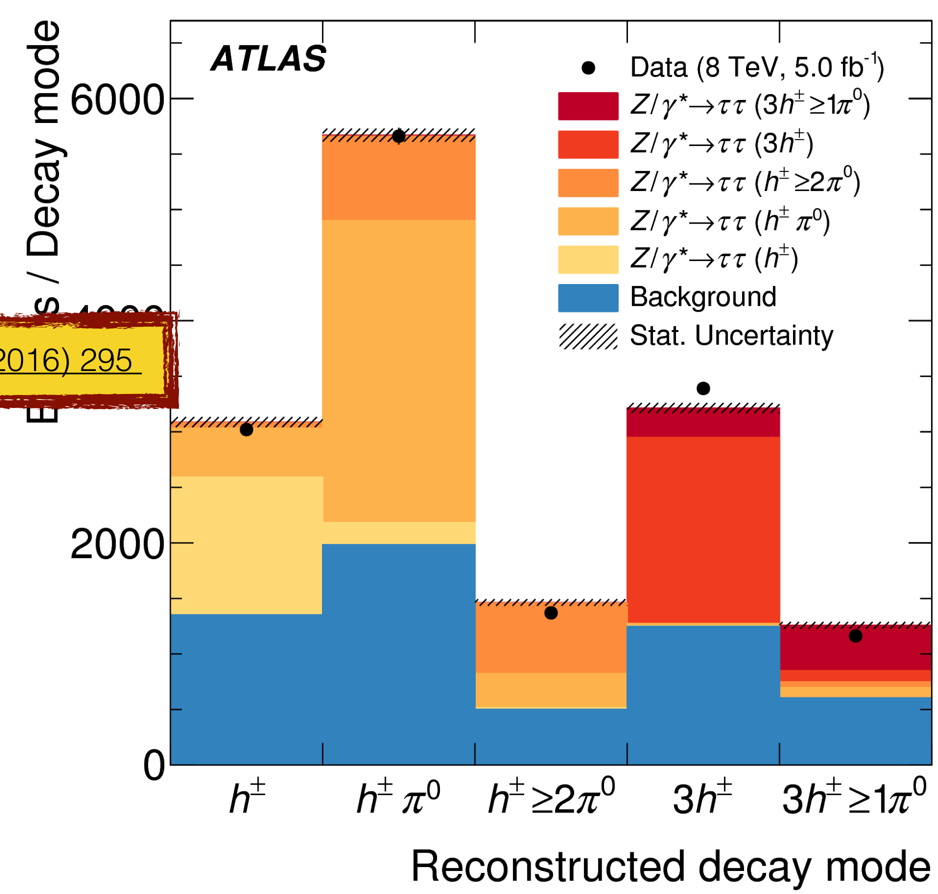

Particle Flow Performance

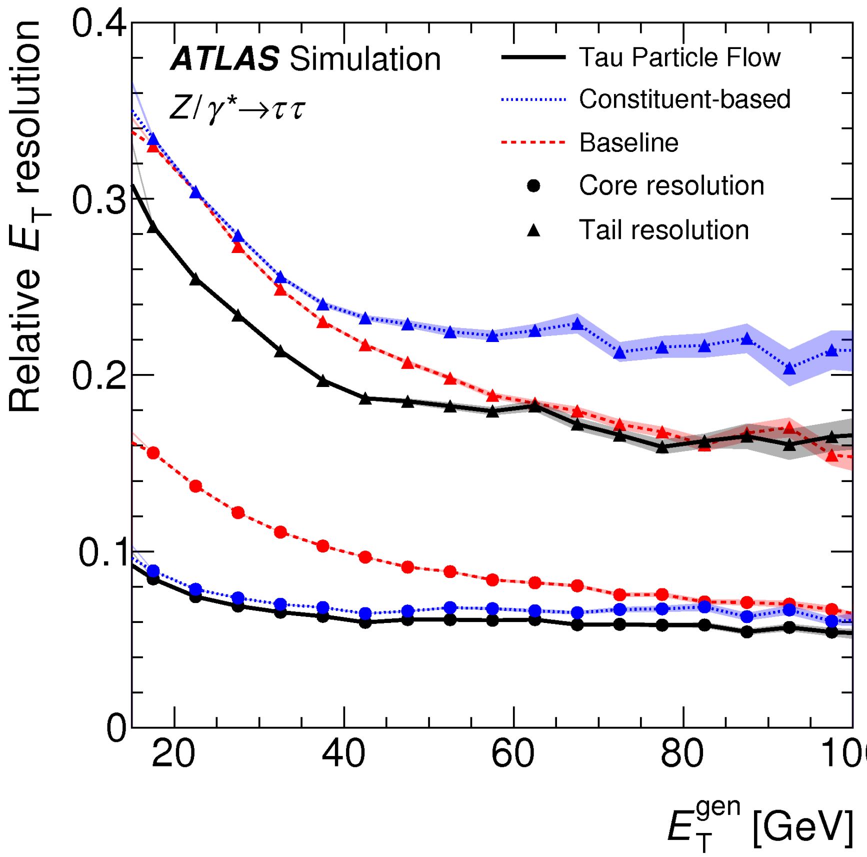

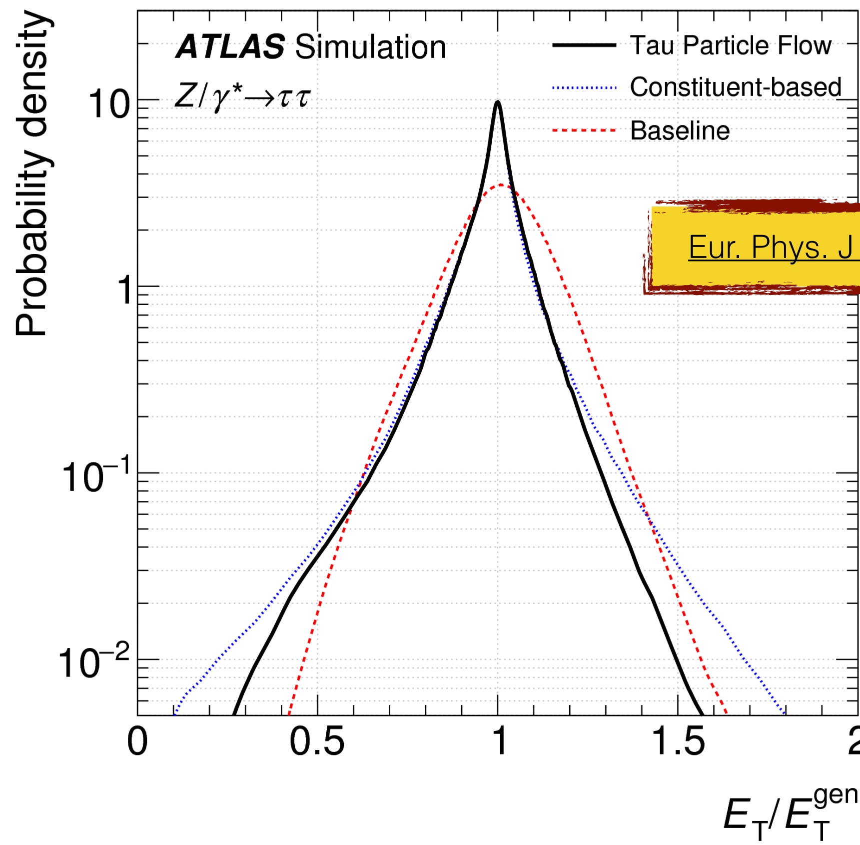

Eur. Phys. J C 76 (2016) 295

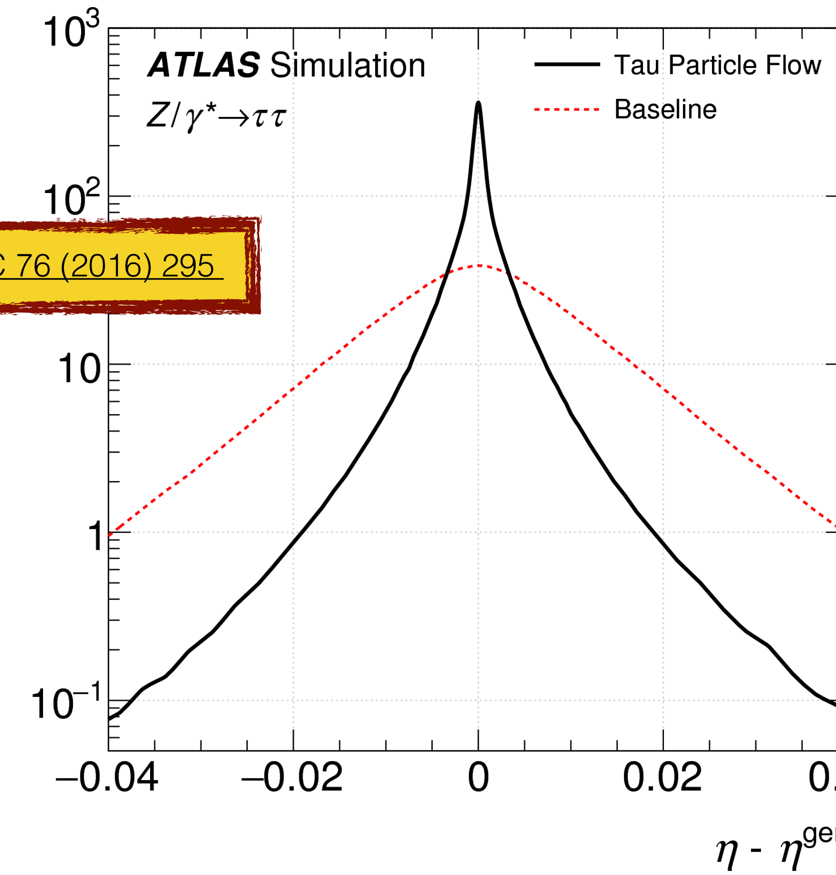

- Tau particle flow provides great improvement over simple calorimeter-based energy measurement
- Final tau energy is determined by boosted regression tree that combines the calo-based and particle flow measurements depending on energy, decay mode, etc.

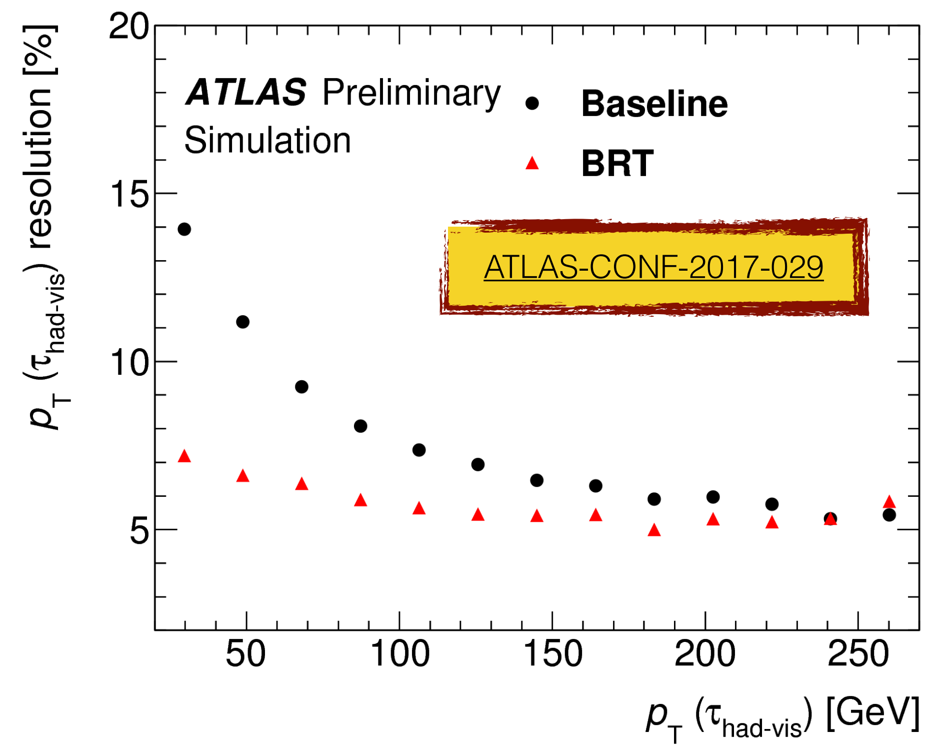

ATLAS-CONF-2017-029

Tau Identification

- Use recurrent NN with LSTM architecture to combine information from individual tracks, clusters and several high-level observables into a single classifier
- Significant improvement over BDT that only used high-level observables
- Performance very robust against pile-up

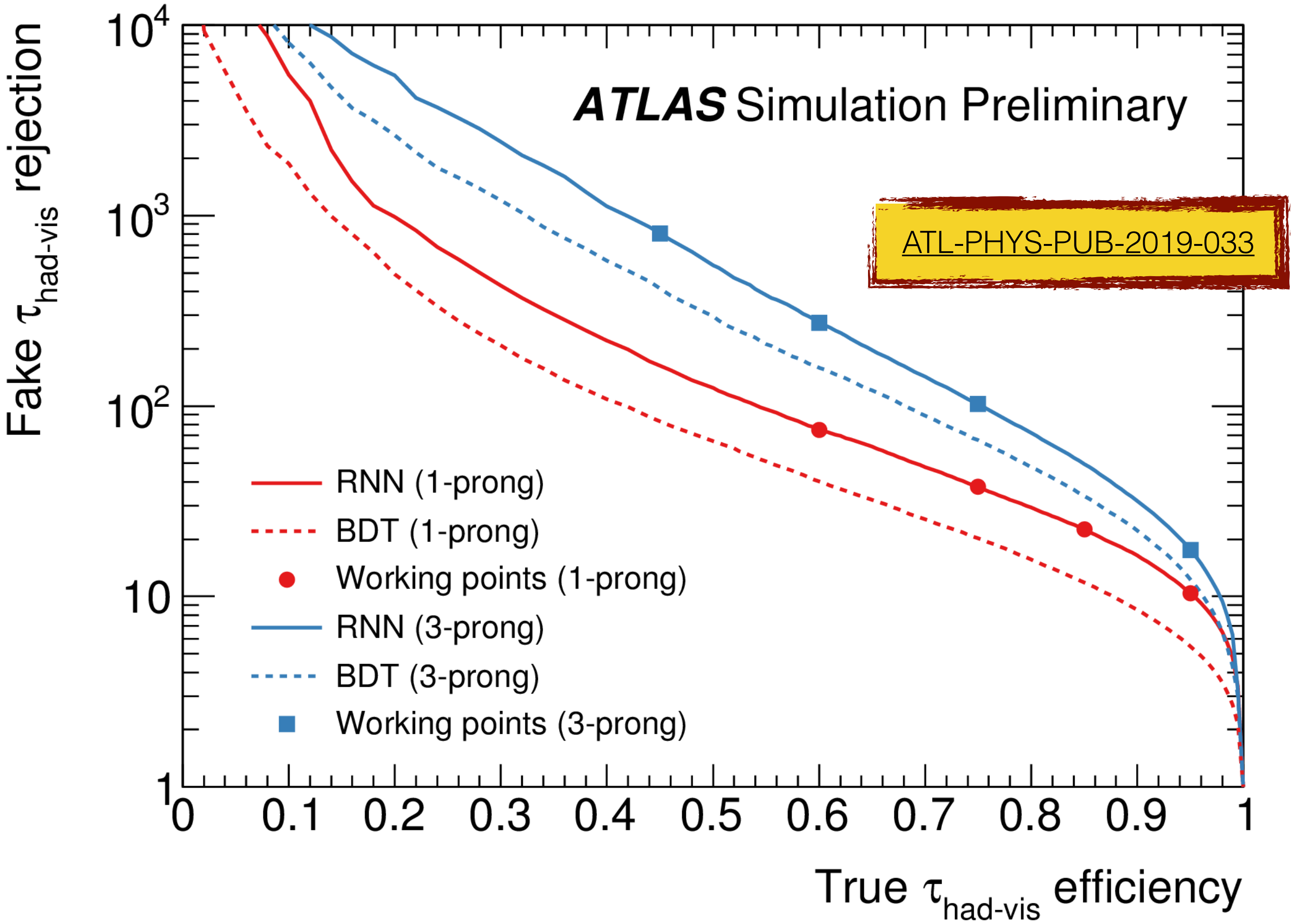

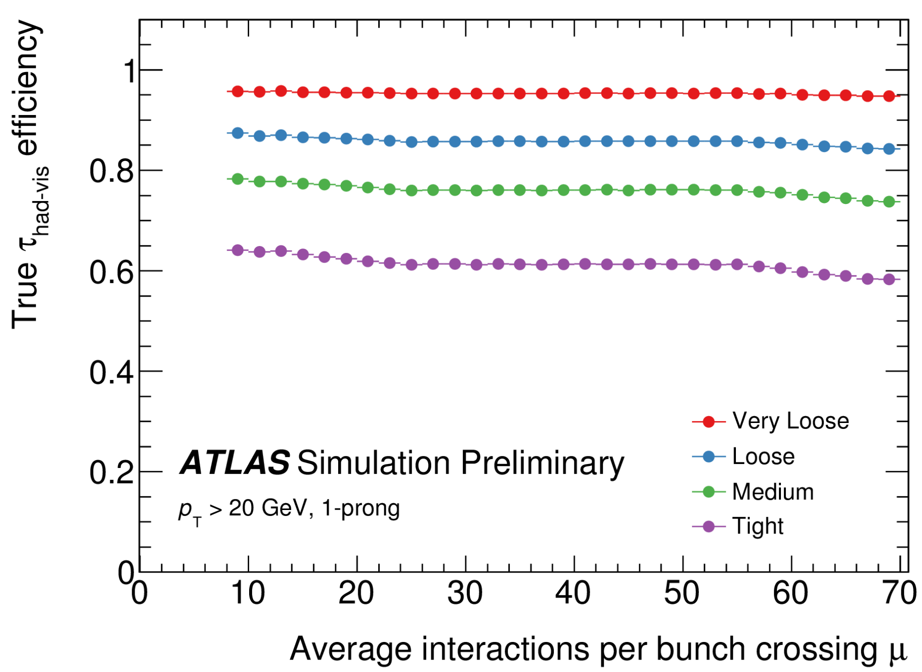

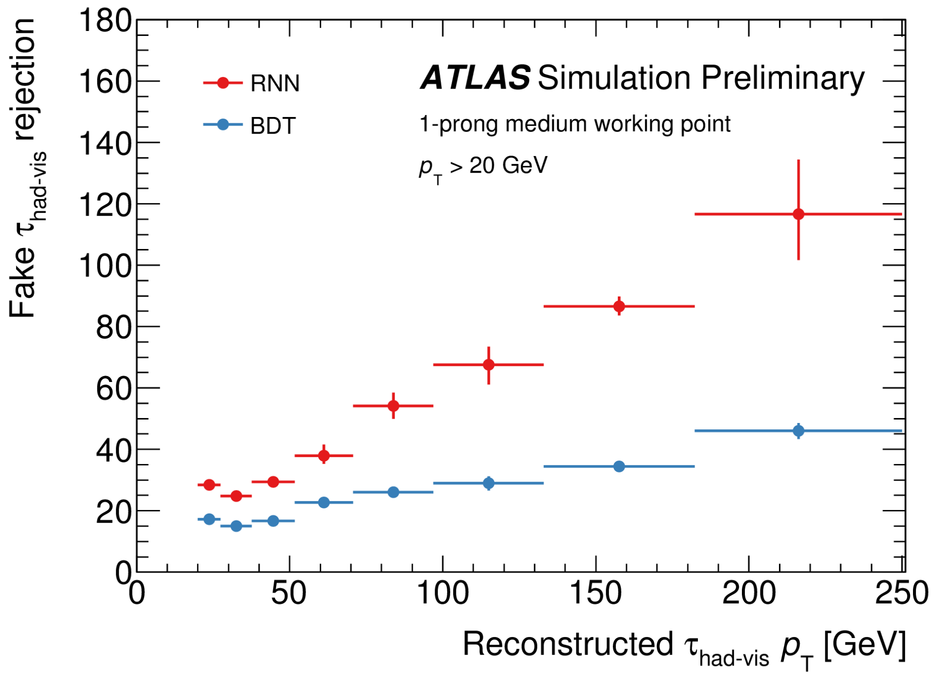

Calibration

ATLAS-CONF-2017-029

- $Z \rightarrow \tau_\mu \tau_{\text{had}}$ provides a clean final state to calibrate the energy scale (1-3%) and identification efficiency (<5%)

- $Z \rightarrow e^+e^-$ allows to measure electron misidentification efficiency

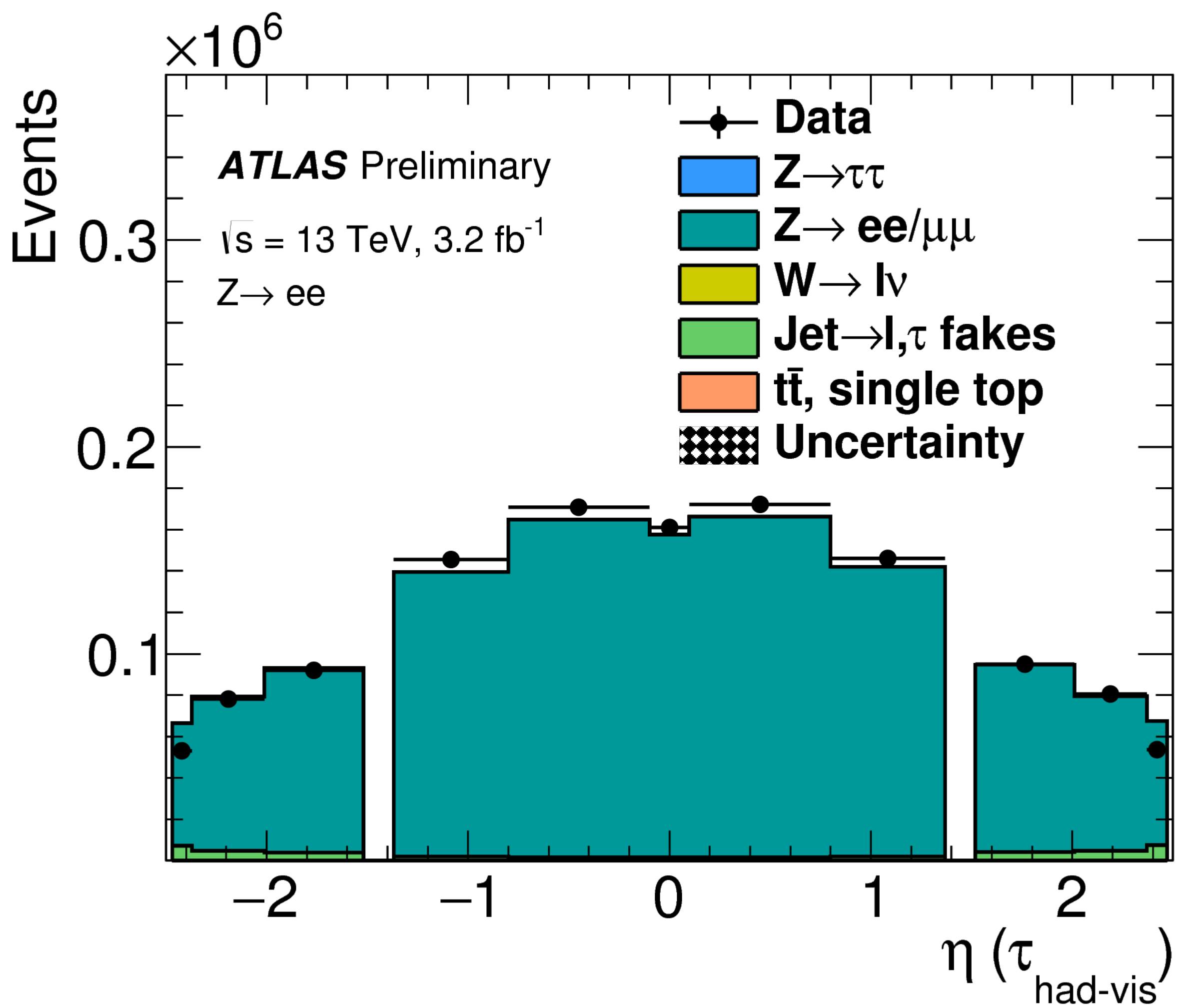

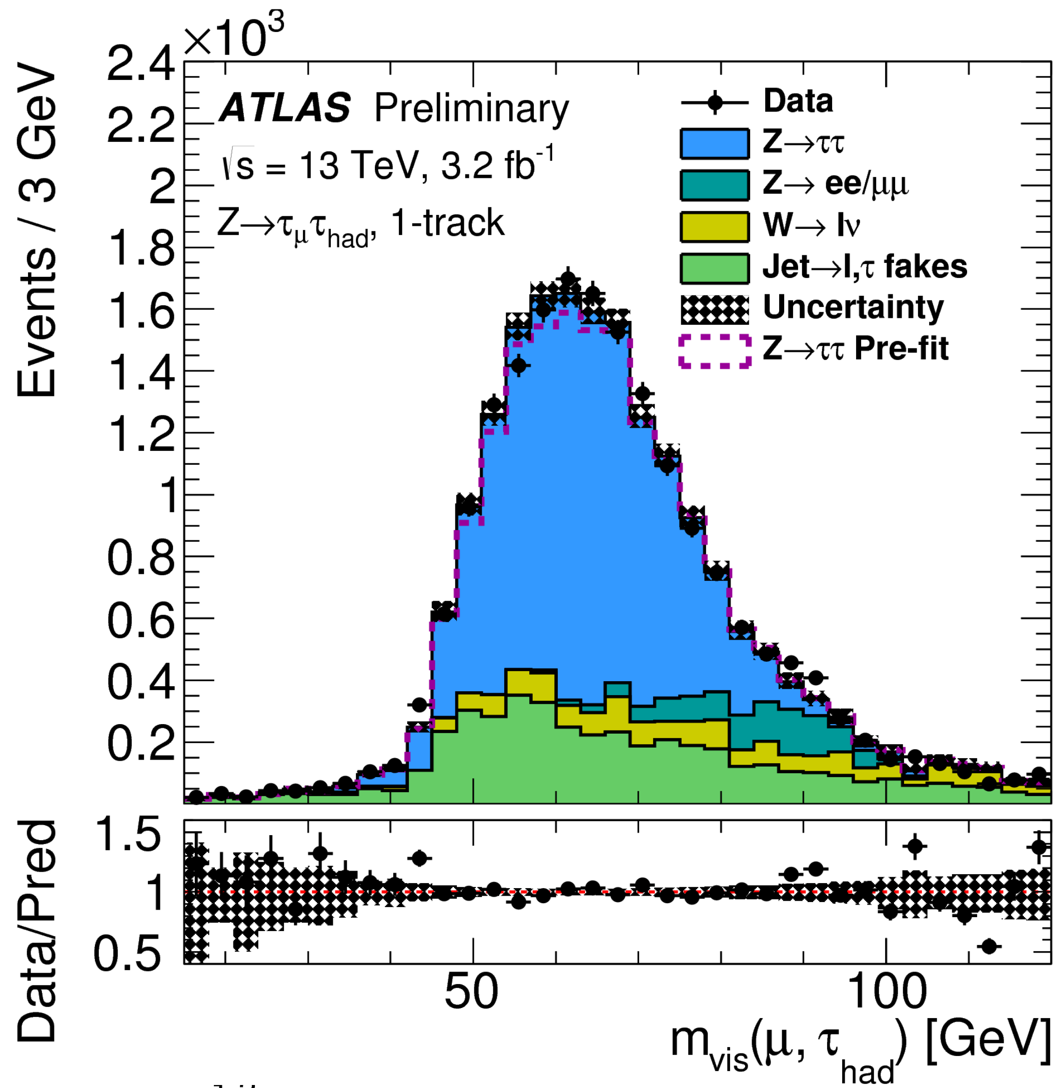

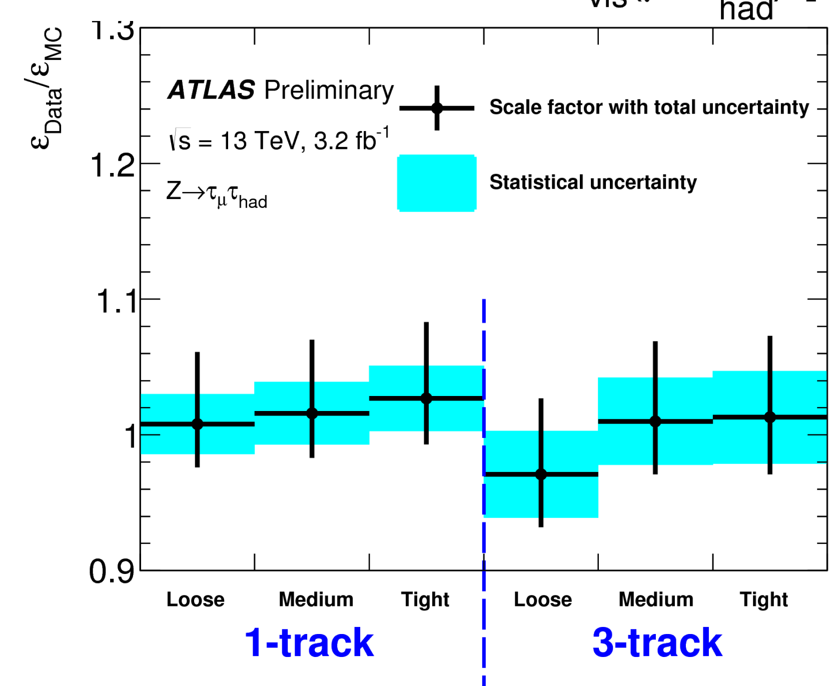

Hadronic Tau Trigger

- L1 Trigger:
  - No track reconstruction
  - Coarse 2x2 calorimeter window
  - Require isolation ring
  - Limited energy resolution leads to slow turn-on cure
- HLT:
  - Simplified version of offline reconstruction
  - Calorimeter-based energy measurement
  - Simpler track reconstruction
  - Simpler tau identification

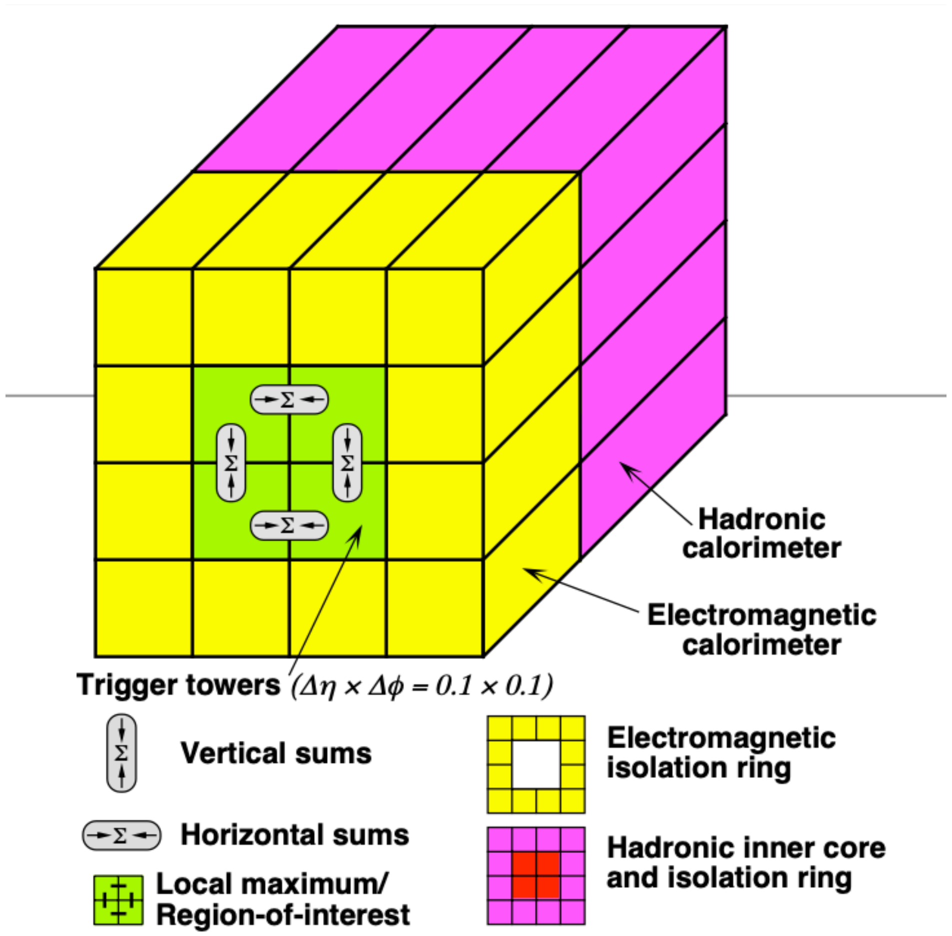

HLT tau trigger step	Mean [ms]	RMS [ms]
Calo-only preselection:		
Topo-clustering	7	3
$\tau_{\text{had-vis}}$ reconstruction	1	0
Track preselection:		
First stage fast tracking	32	16
Second stage fast tracking	27	14
$\tau_{\text{had-vis}}$ reconstruction	1	0
Offline-like selection:		
Precision tracking	21	12
$\tau_{\text{had-vis}}$ reconstruction and BDT	1	0

ATLAS EXPERIMENT

Tau Trigger Menu

UNIVERSITÄT BONN

ATLAS-CONF-2017-061

- Single tau, di-tau and tau+X triggers are available
- Di-tau triggers require additional jet at L1 to achieve acceptable rate

Trigger	Typical offline selection	Trigger selection		Trigger rate at 1.2×10^{34} cm^{-2}s^{-1}	
		L1	HLT	L1 [kHz]	HLT [Hz]
τ	$p_T^\tau > 170$ GeV	60	160	5.2	15
2τ	$p_T^\tau > 40, 30$ GeV, $p_T^{jet} > 80$ GeV	20i,12i,25	35,25,-	6.7	35
τ+e	isolated e, $p_T^e > 18$ GeV, $p_T^\tau > 30$ GeV, $p_T^{jet} > 80$ GeV	15i,12i,25	17i,25,-	3.4	9
$\tau+\mu$	isolated μ, $p_T^\mu > 15$ GeV, $p_T^\tau > 30$ GeV, $p_T^{jet} > 80$ GeV	10,12i,25	14i,25,-	1.7	7
$\tau+E_T^{miss}$	$p_T^\tau > 40$ GeV, $E_T^{miss} > 150$ GeV, $p_T^{jet} > 70$ GeV	20i,45,20	35,70,-	1.8	8
2τ with L1Topo	$p_T^\tau > 40, 30$ GeV, $\Delta R(\tau,\tau) < 2.6$	20i,12i,2.9	35,25,-	5.9	39
	$p_T^\tau > 40, 30$ GeV, $\Delta R(\tau,\tau) < 2.6$, $p_T^{jet} > 80$ GeV	20i,12i,2.9,25	35,25,-,-	3.8	24

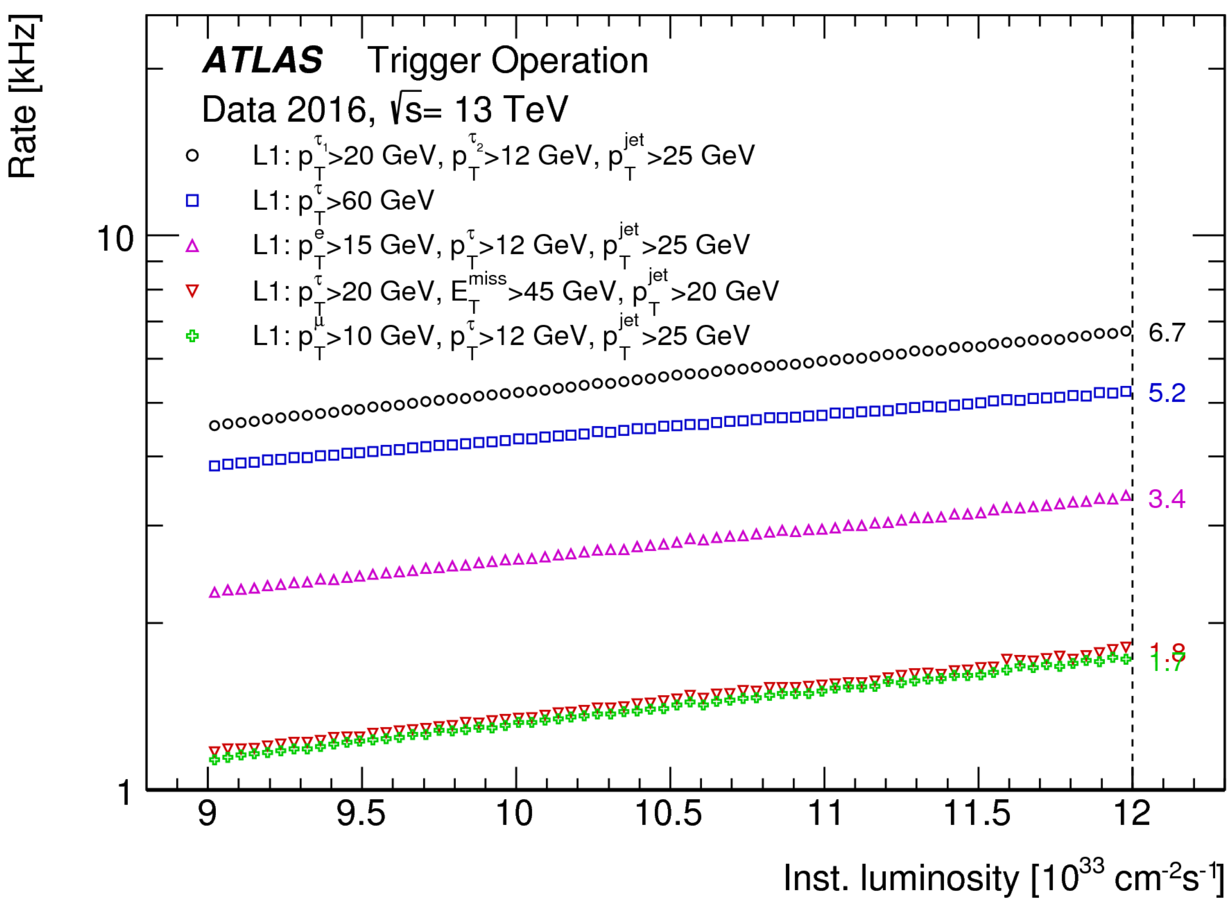

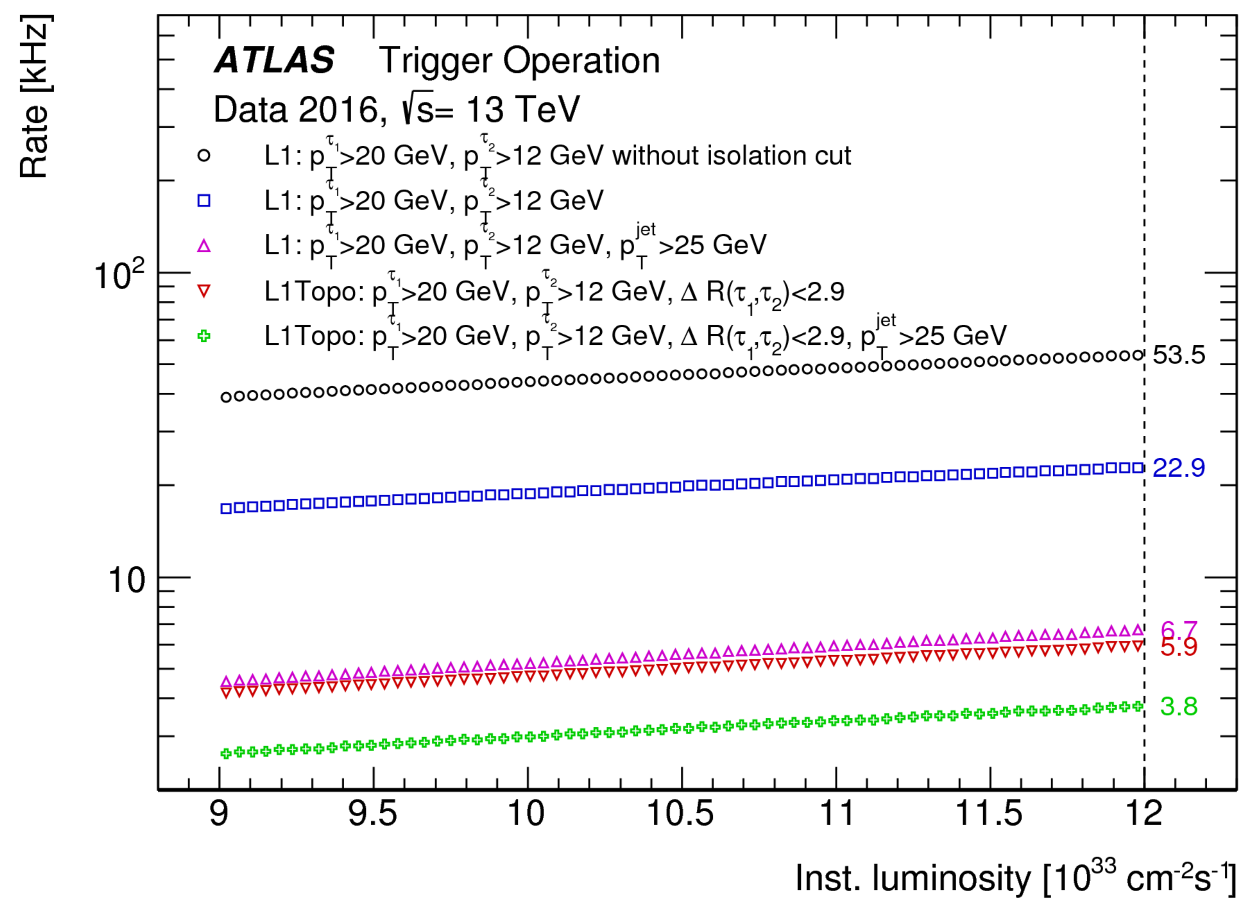

Tau Trigger Efficiency

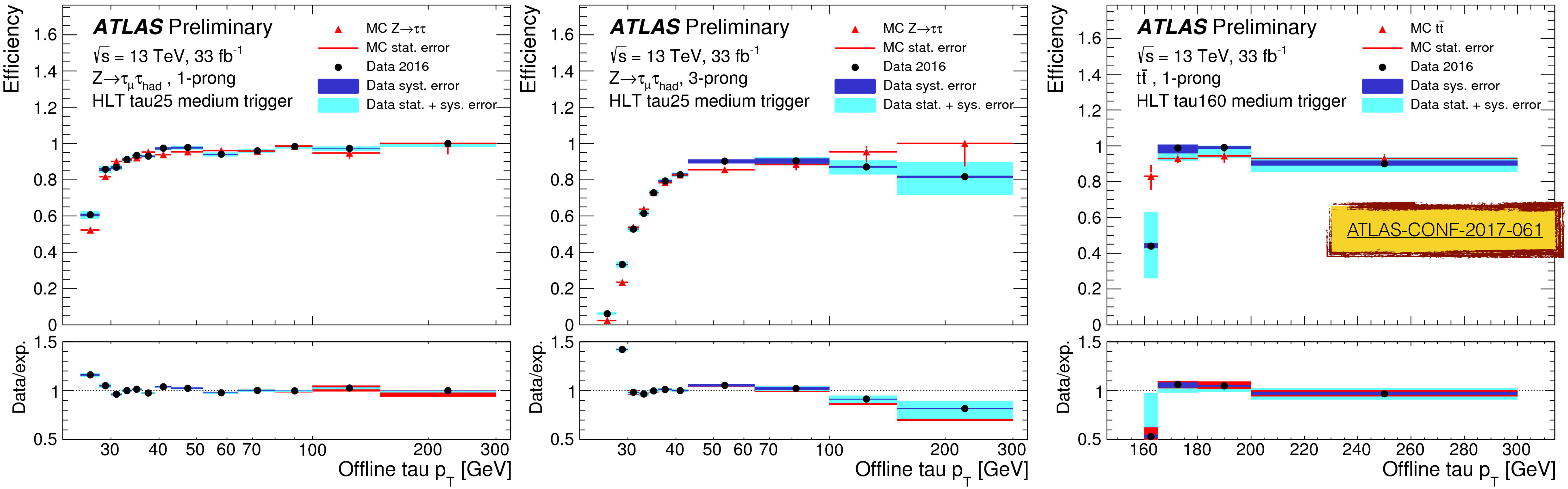

- Trigger efficiencies are measured using $Z \to \tau_\mu \tau_{\mathrm{had}}$ for low p_{T} and $t\bar{t} \to b\bar{b}\mu\nu_\mu\tau_{\mathrm{had}}\nu_\tau$ for high p_{T} τ-leptons
- Use independent muon trigger in both cases to select events
- Trigger turn-on well modelled in simulation, efficiency measured with 1-10% precision

Calorimeter Response with $W \rightarrow \tau^{\pm}\nu$

- Calibration of the response in the hadronic calorimeter from isolated pion tracks in MinBias events (low p_{T}) and test beam data taken at the SPS ($p_{\mathrm{T}} < 350$ GeV)
- New measurement using isolated high p_{T} pions from $W \rightarrow \tau^{\pm}(\rightarrow \pi^{\pm}\nu_{\tau})\nu_{\tau}$ decays allows calibration up to several 100 GeV using pp collision data
- Select isolated tracks with large d_0 and $E_{\mathrm{T}}^{\mathrm{miss}} > 150$ GeV. Sum of calorimeter energy within $\Delta R < 0.15$ around track after correction for average pile-up
- Extract mean and width of peak in E/p distribution

arXiv:2108.09043

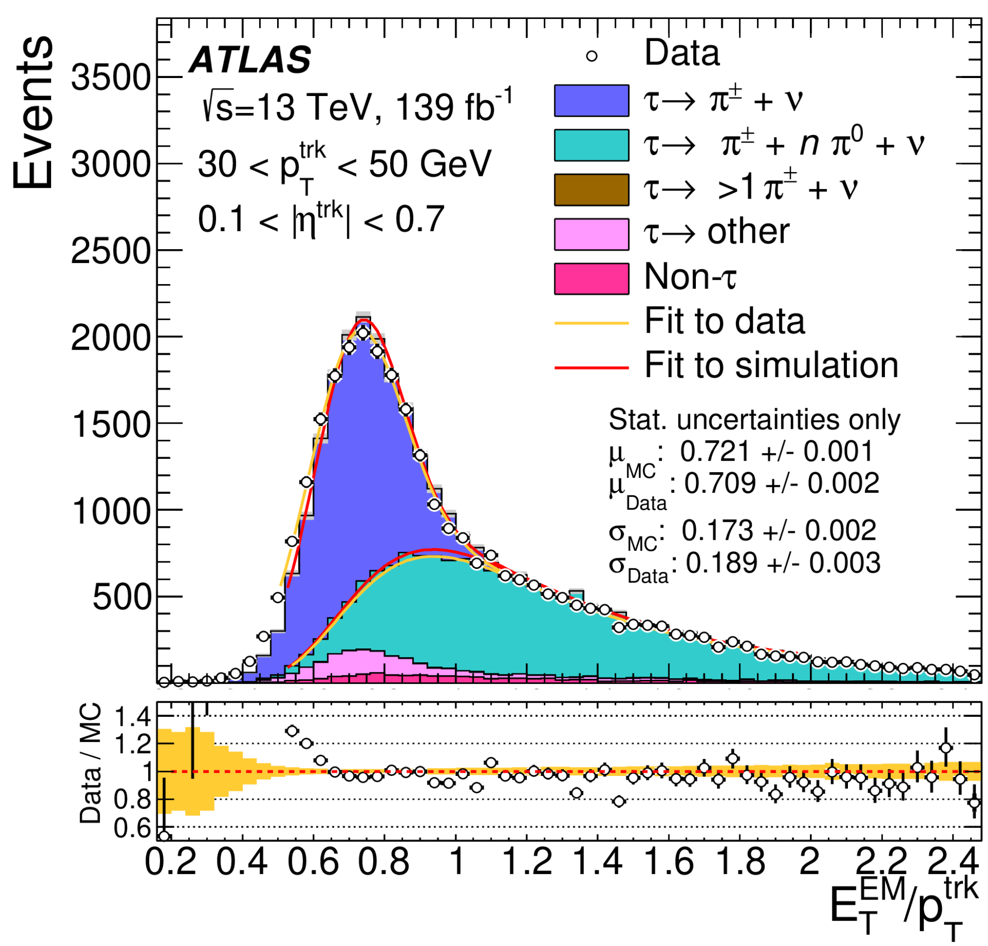

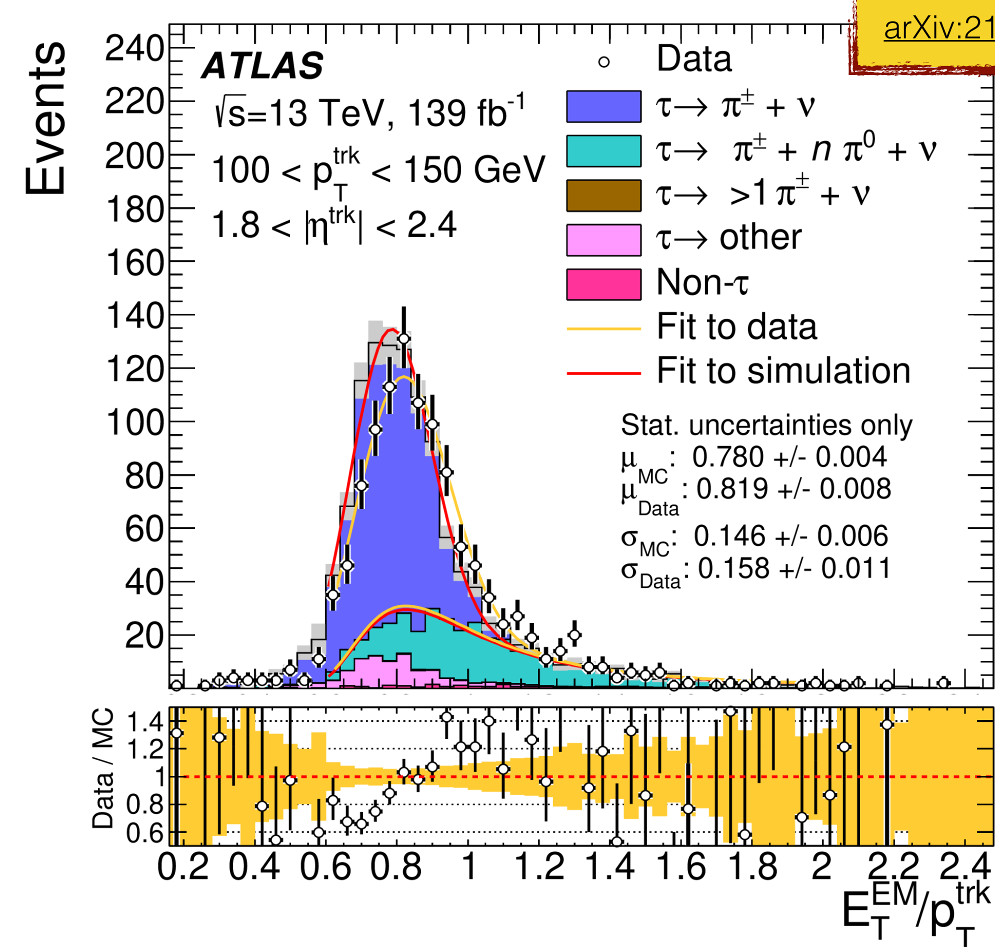

Calorimeter Response with $W \to \tau^{\pm}\nu$

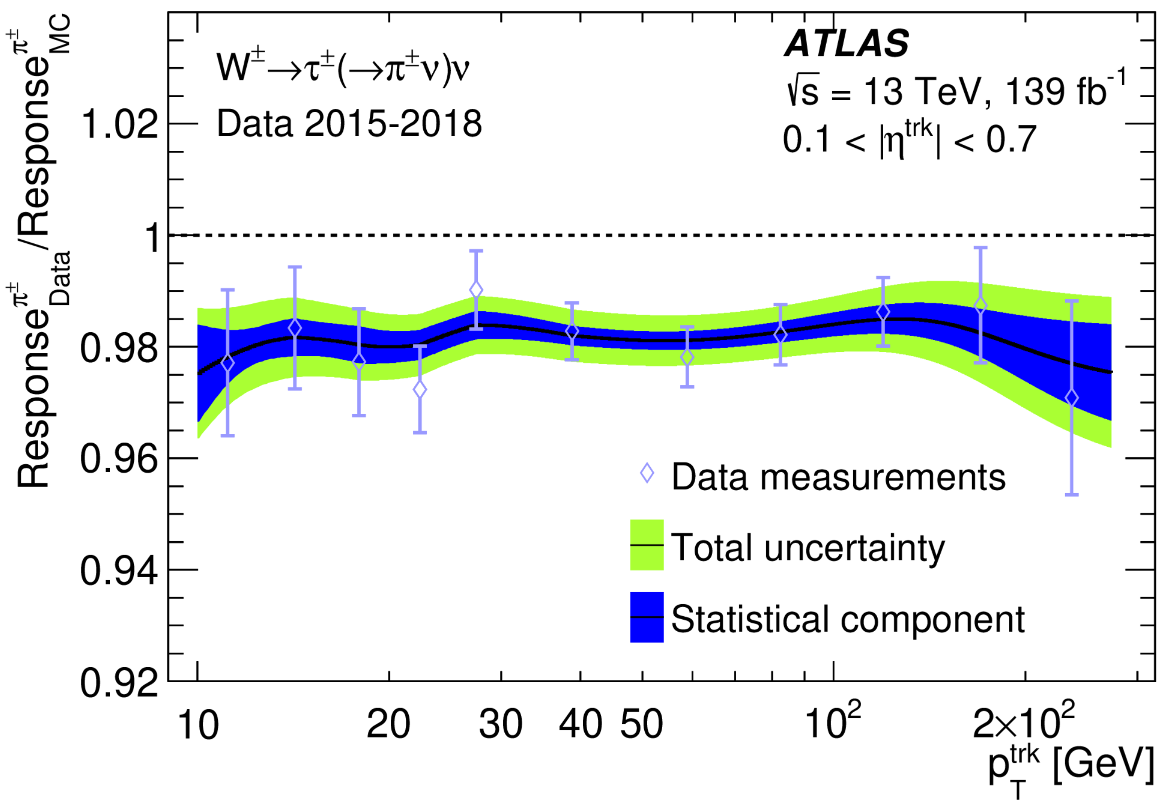

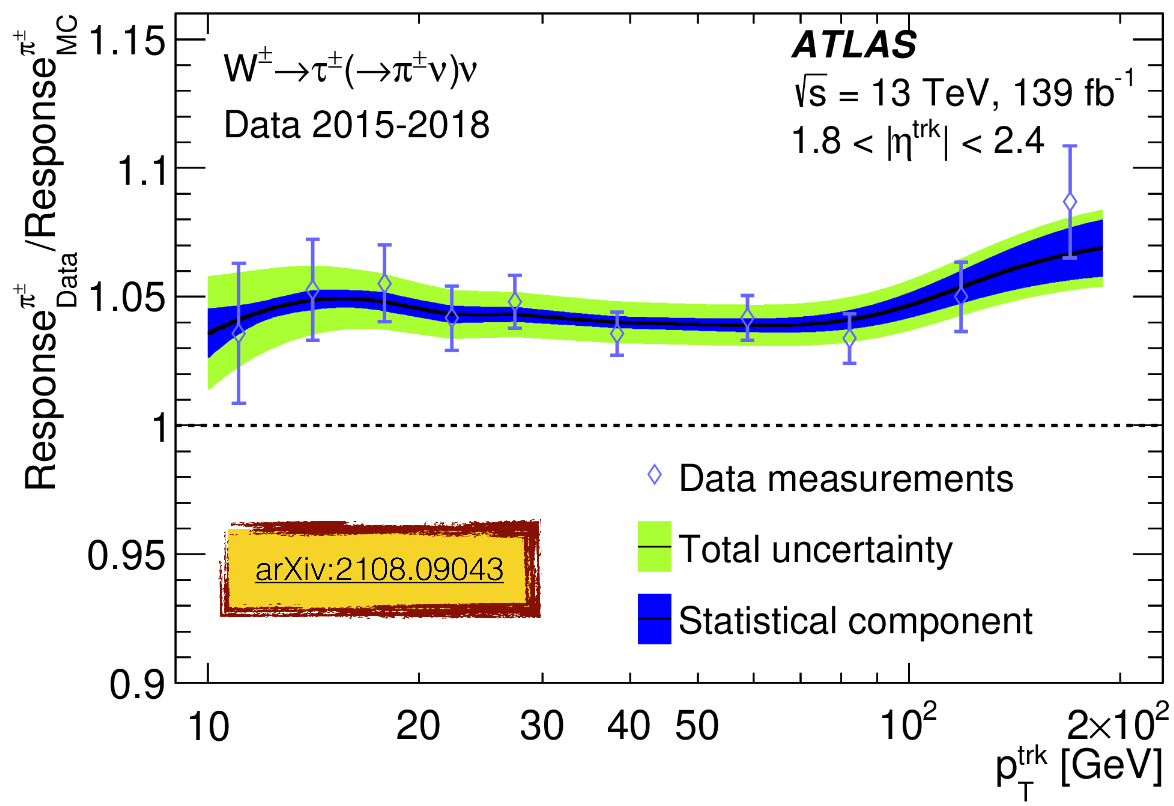

- Measured single hadron response E/p, width of E/p and longitudinal energy distribution over large p_{T} range and depending on η

- Allows to validate and improve the simulation of the hadronic calorimeter response in ATLAS

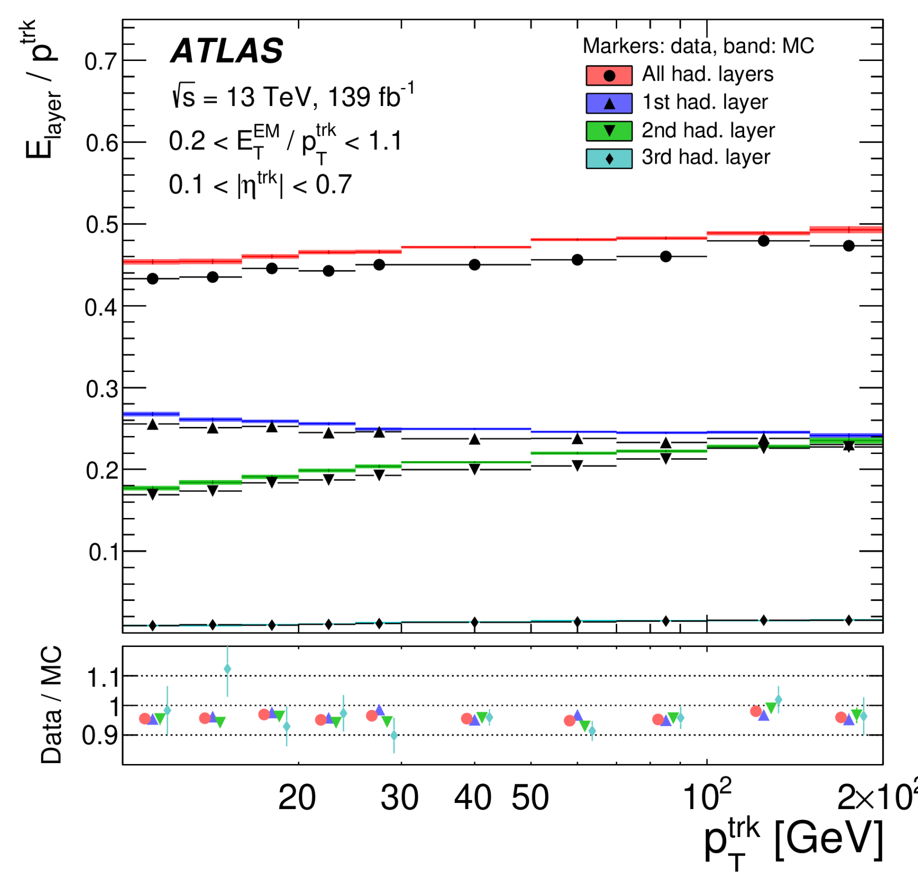

Boosted Di-Tau Systems

- Boosted di-tau systems fail the standard tau reconstruction due to the R=0.4 seed jets
- Dedicated reconstruction starting from anti-k_T jets with R=1.0 and $p_T > 300$ GeV; identify R=0.2 sub-jets that correspond to two hadronic τ-lepton decays
- Dedicated BDT using similar input as the single tau ID is used to reject fake tau backgrounds

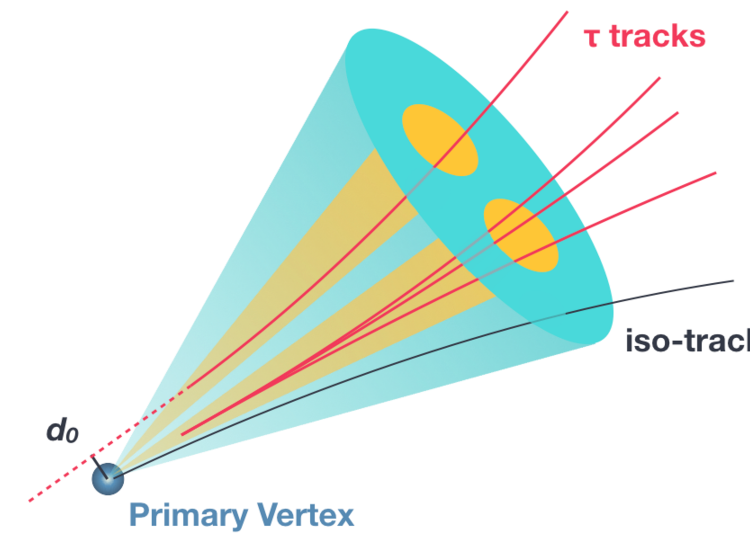

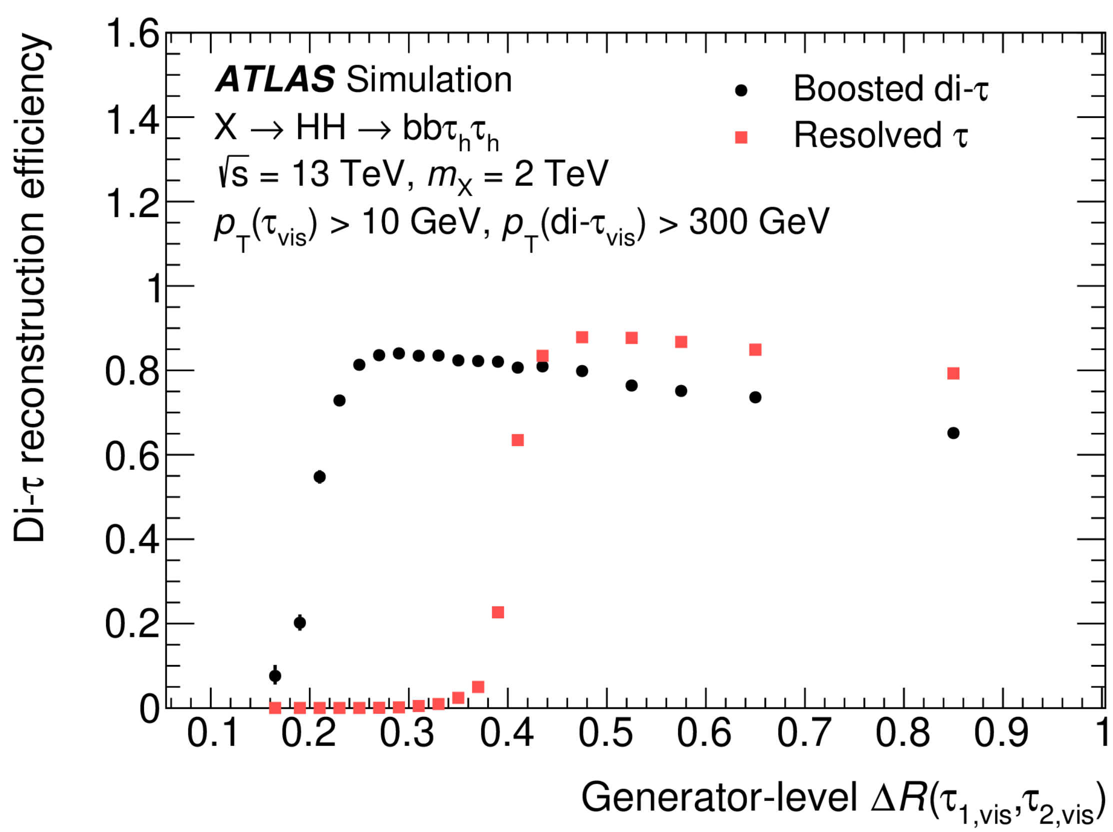

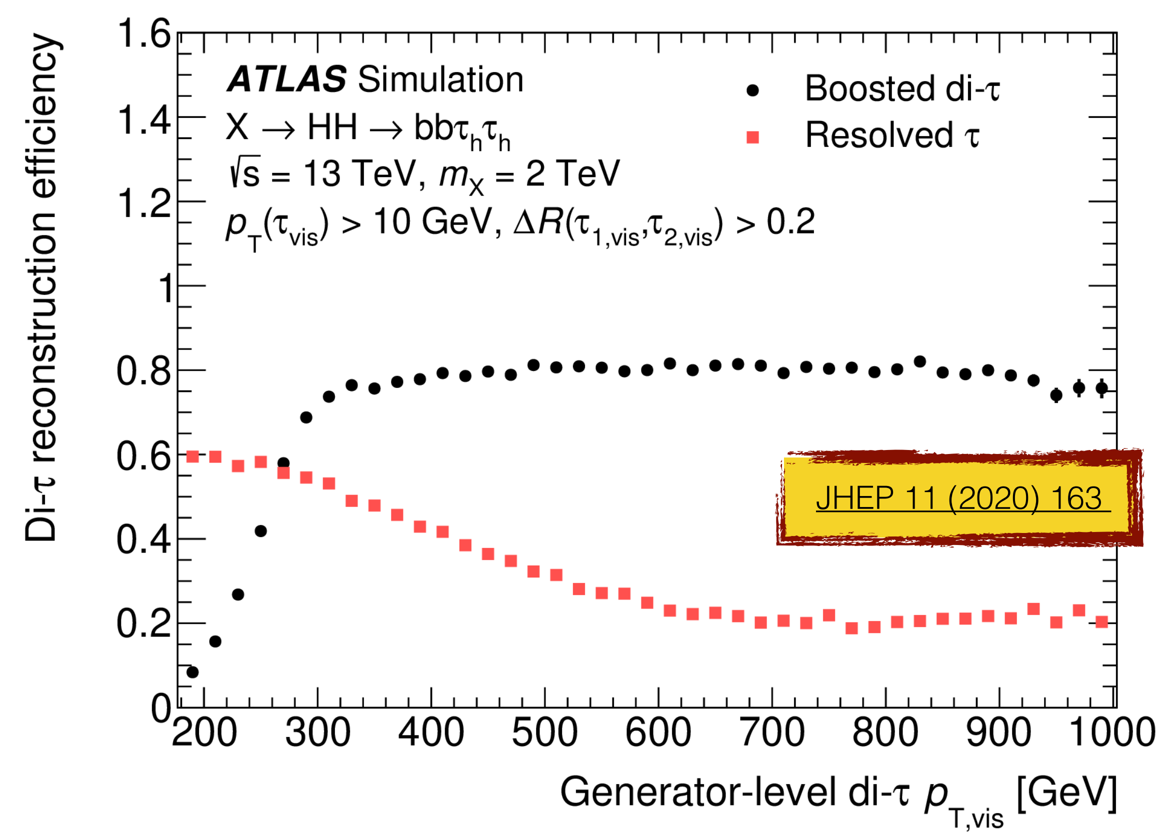

JHEP 11 (2020) 163

Boosted Di-Tau Systems

JHEP 11 (2020) 163

- Use boosted $Z \to \tau\tau$ events to calibrate selection and reconstruction efficiency
- Can be used to search for heavy resonances like $HH \to b\bar{b}\tau^+\tau^-$ up to very high masses
- Trigger on large-R jet from boosted $b\bar{b}$ or $\tau^+\tau^-$ system

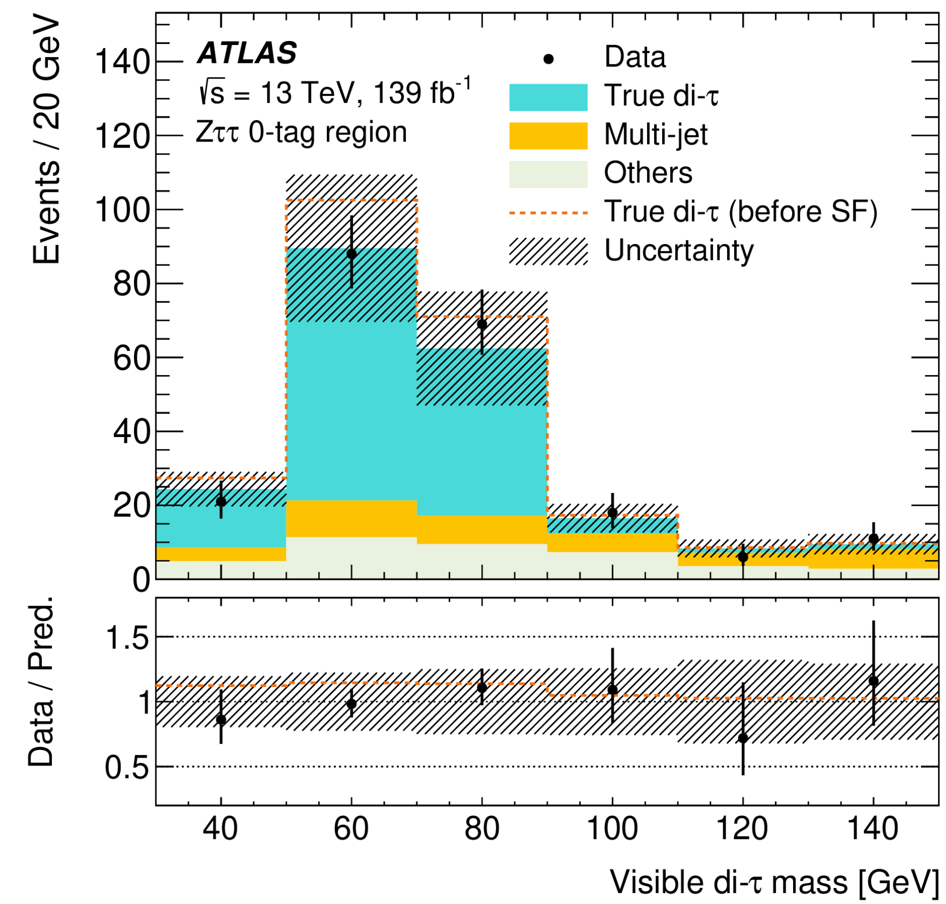

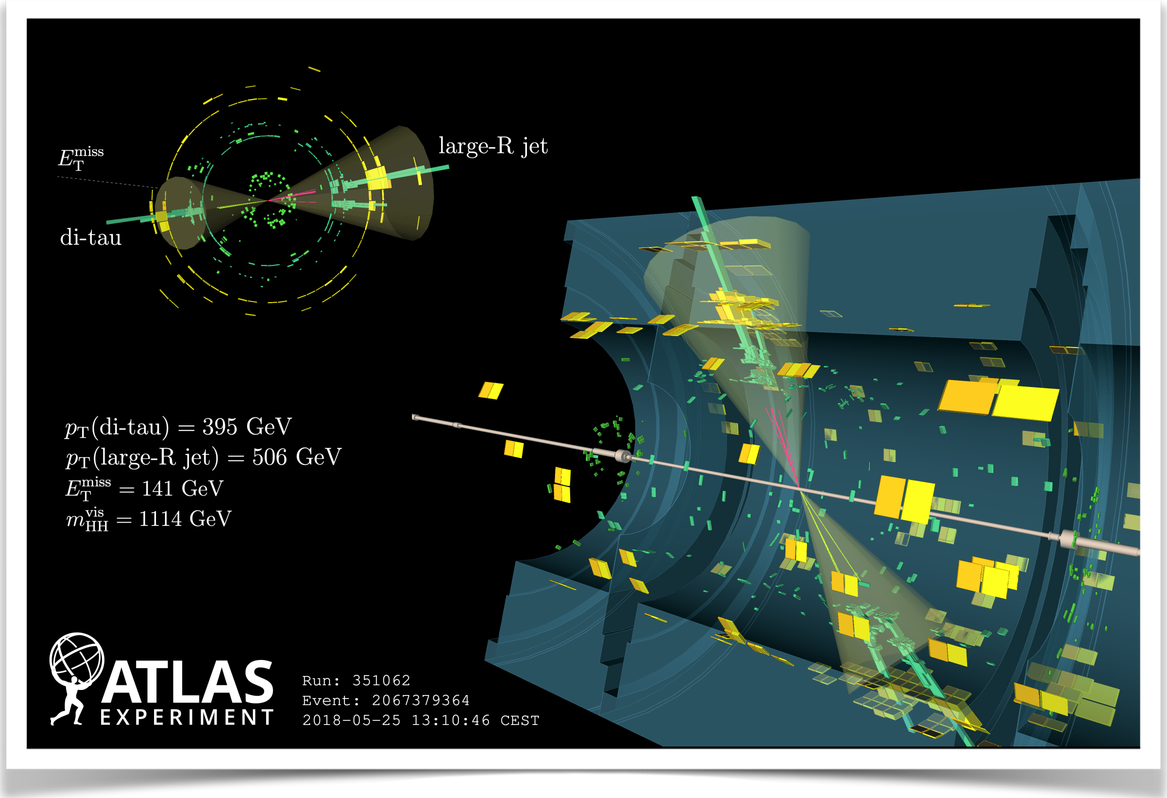

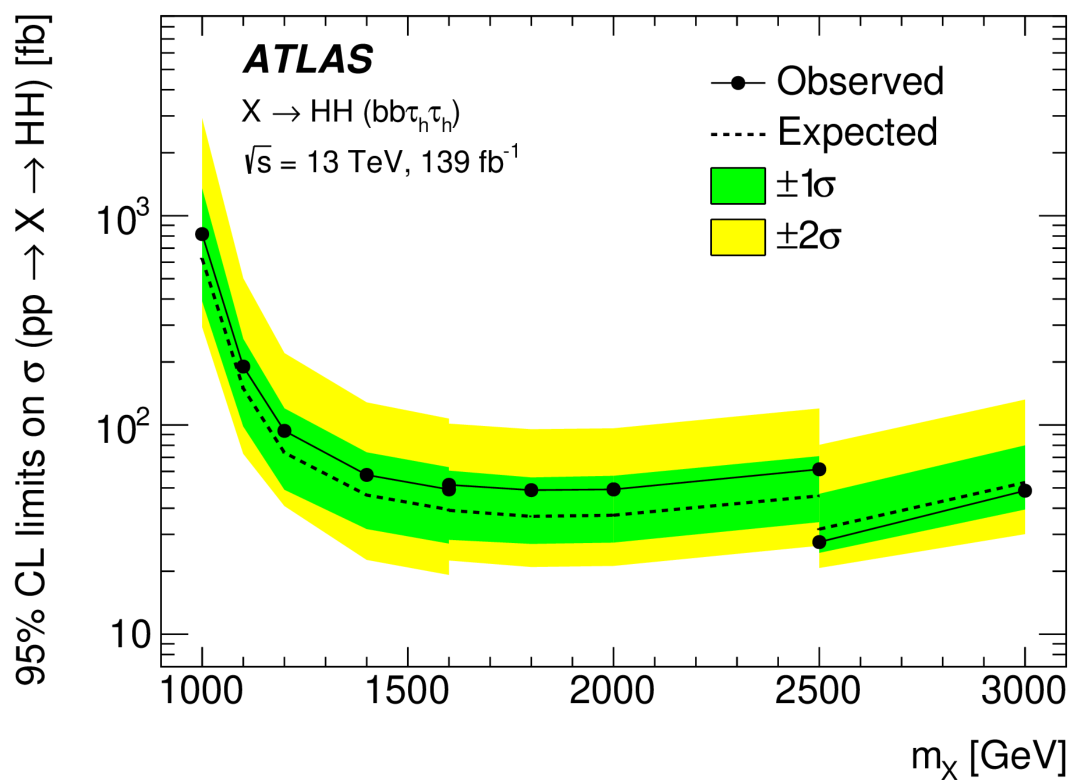

Selected Measurements using Taus

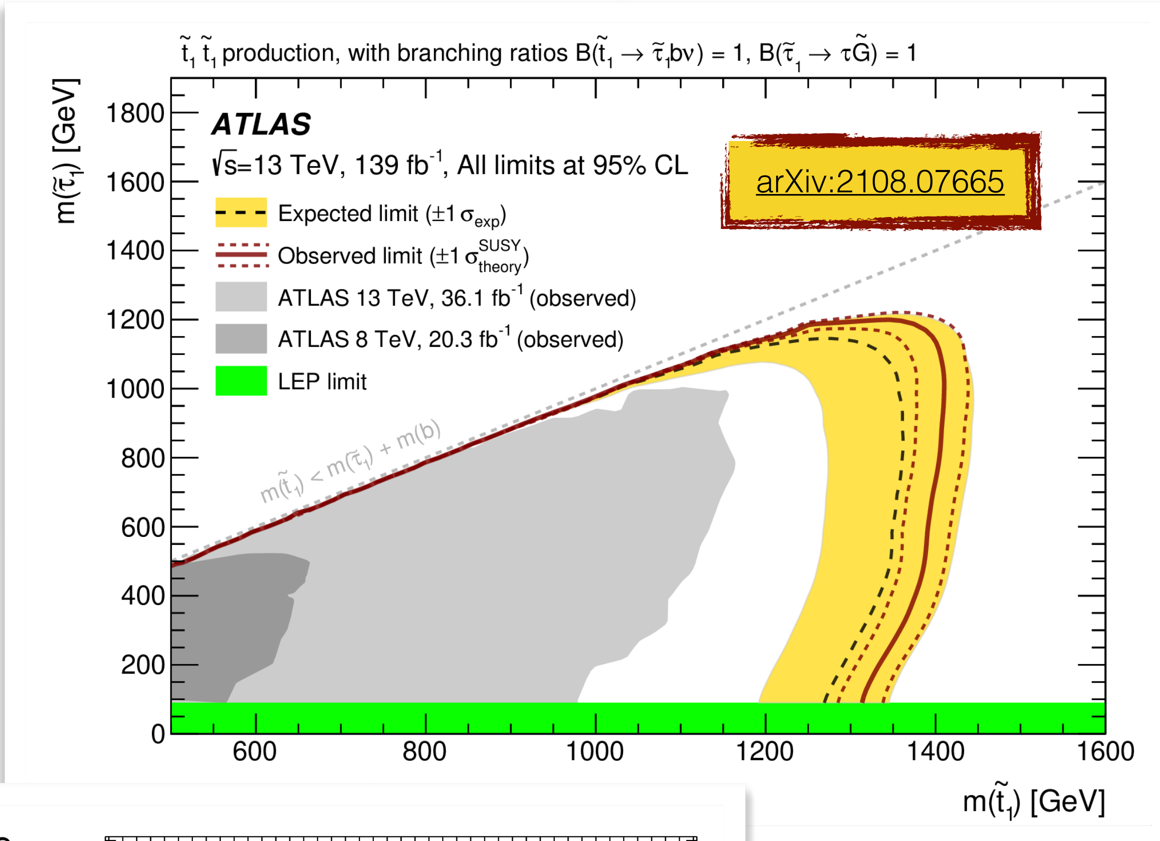

arXiv:2108.07665

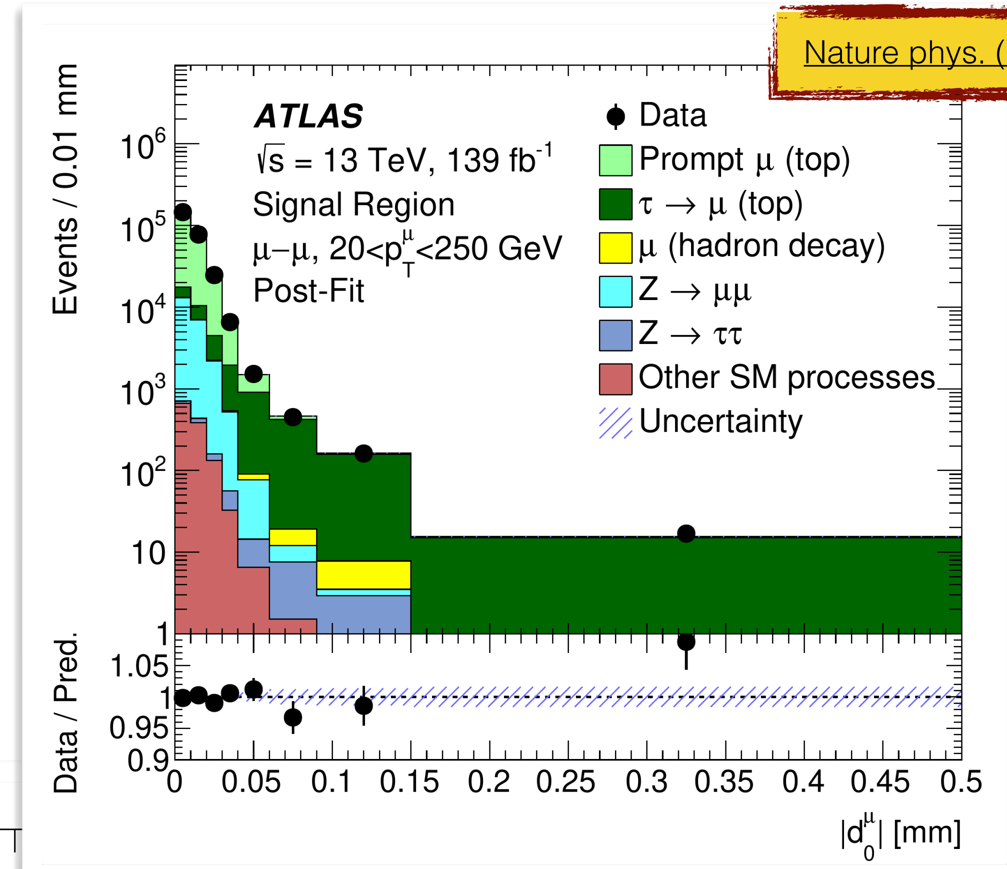

Nature phys. (2021)

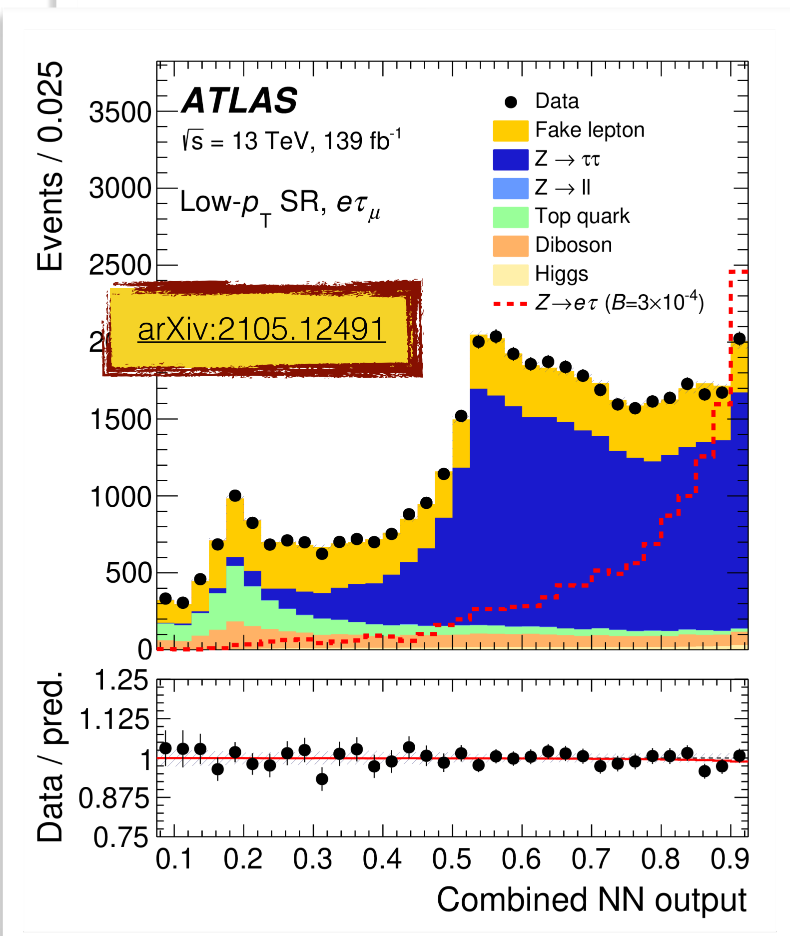

arXiv:2105.12491

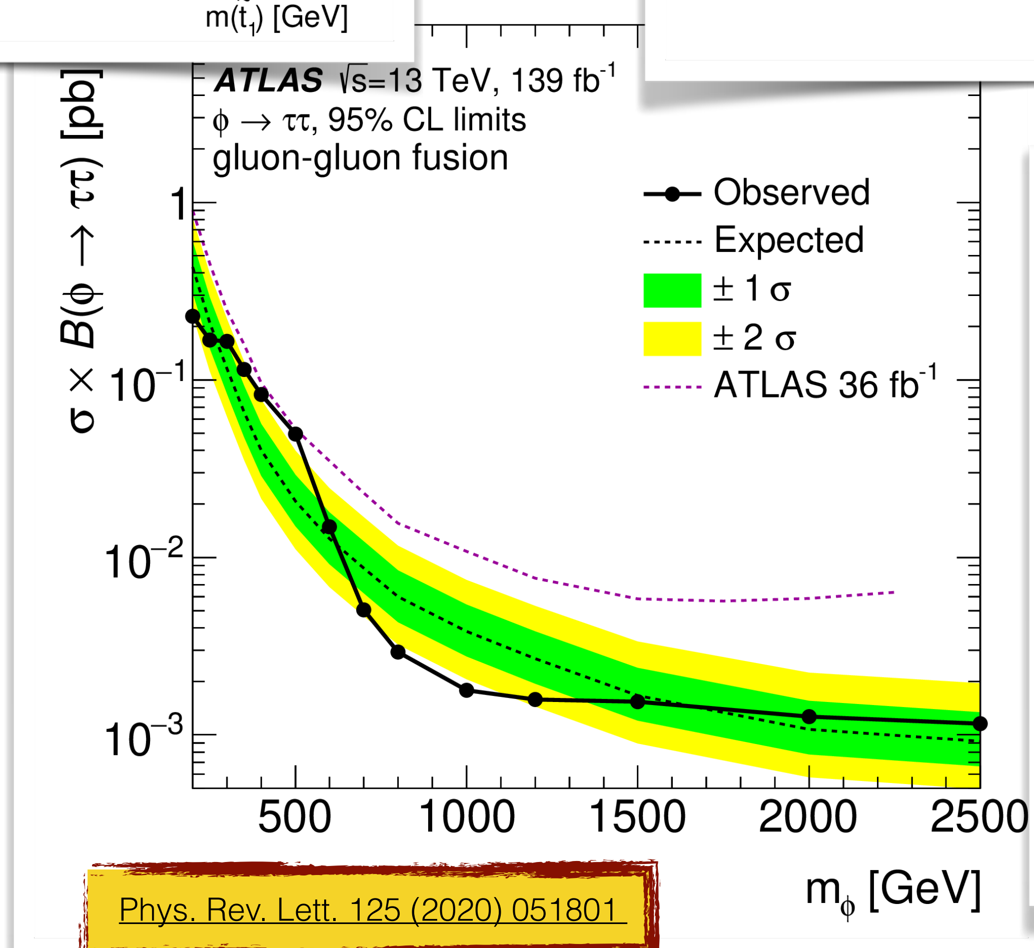

Phys. Rev. Lett. 125 (2020) 051801

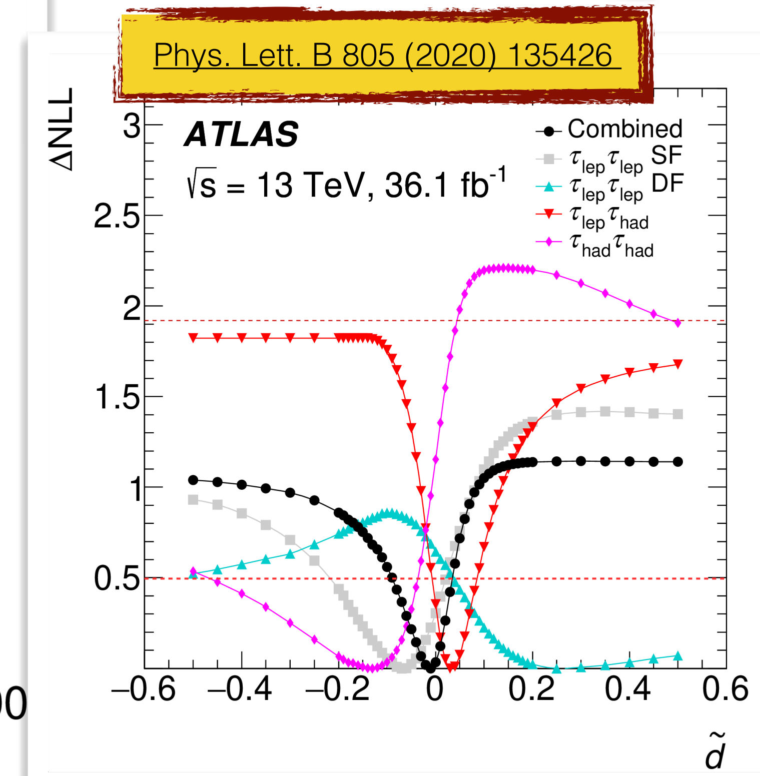

Phys. Lett. B 805 (2020) 135426

Conclusions

- Machine learning techniques allow for excellent reconstruction of hadronic τ-lepton decays even at high pile-up conditions
- Reconstruction and identification techniques are being developed further and will be available in re-reconstruction of ATLAS data
- Reports on recent measurements using τ-leptons in ATLAS at this conference:
  - Lepton Flavor Violation Searches at ATLAS and CMS - Luca Fiorini
  - Searches for new physics with leptons using the ATLAS detector - Matteo Franchini
  - Searches for leptoquarks with the ATLAS detector - Zhiyuan Li
  - Higgs boson measurements in couplings to tau leptons with the ATLAS experiment - Christopher Young

Backup

Tau Trigger

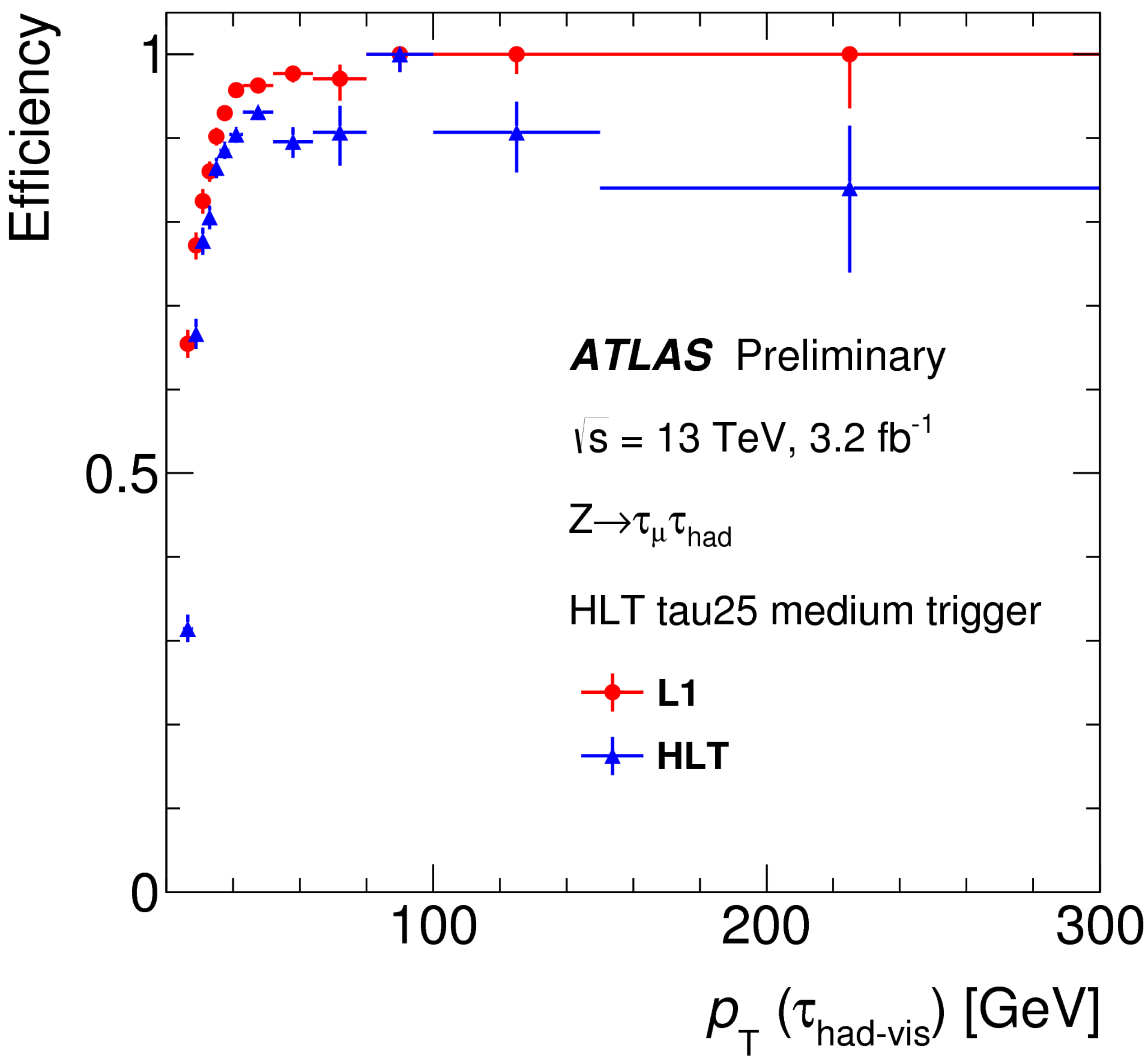

Efficiency
1
0.5
0
100
200
300
ATLAS Preliminary
√s = 13 TeV, 3.2 fb-1
Z→τμτhad
HLT tau25 medium trigger
L1
HLT
pT (τhad-vis) [GeV]

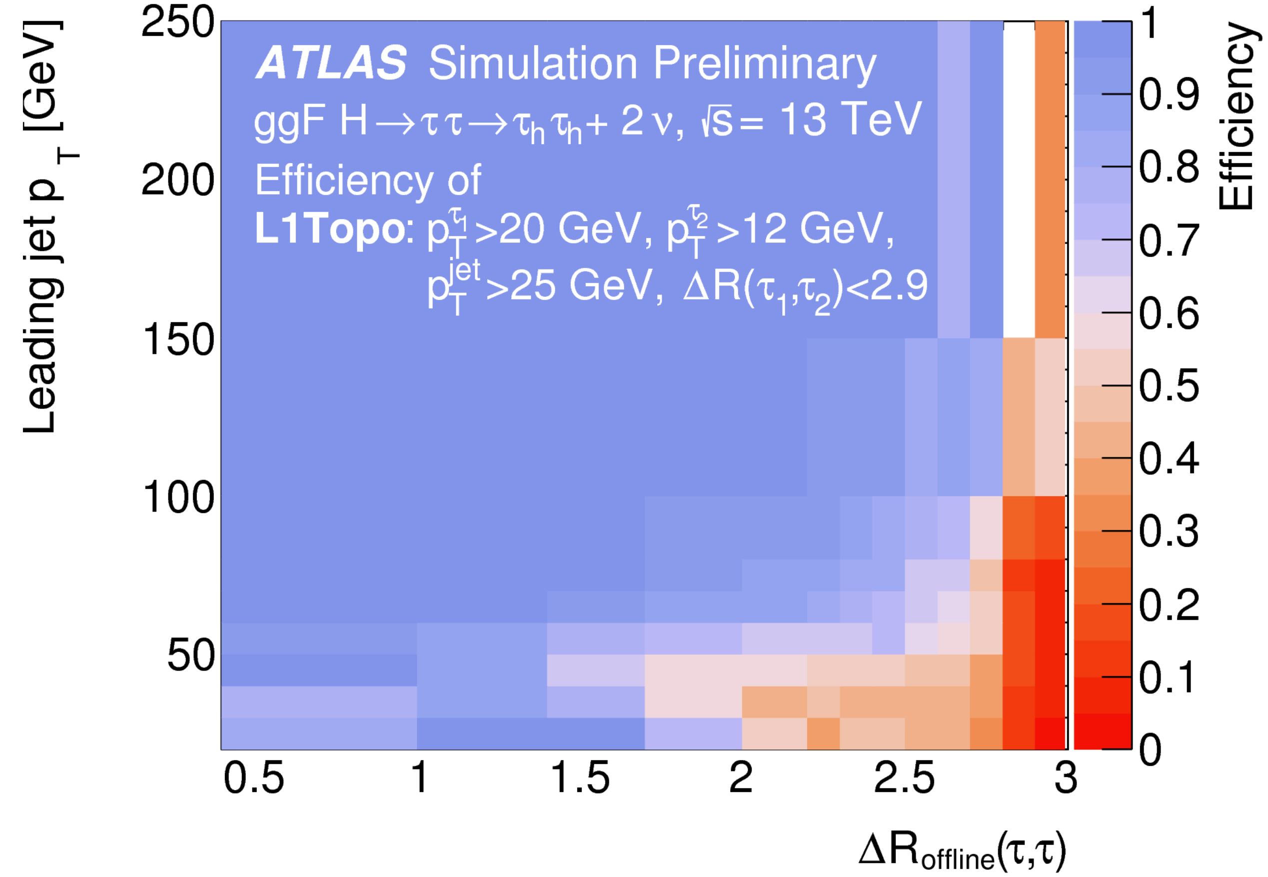

ATLAS Simulation Preliminary
ggF H→ττ→τhτh+ 2ν, √s= 13 TeV
Efficiency of
L1Topo: pTτ1>20 GeV, pTτ2>12 GeV,
pTjet>25 GeV, ΔR(τ1,τ2)<2.9
Leading jet pT [GeV]
250
200
150
100
50
0.5
1
1.5
2
2.5
3
ΔRoffline(τ,τ)
Efficiency
1
0.9
0.8
0.7
0.6
0.5
0.4
0.3
0.2
0.1
0

π^0 identification

Cluster pseudorapidity, $|\eta^{\mathrm{clus}}|$
Magnitude of the energy-weighted η position of the cluster

Cluster width, $\langle r^2 \rangle^{\mathrm{clus}}$
Second moment in distance to the shower axis

Cluster η width in EM1, $\langle \eta^2_{\mathrm{EM1}} \rangle^{\mathrm{clus}}$
Second moment in η in EM1

Cluster η width in EM2, $\langle \eta^2_{\mathrm{EM2}} \rangle^{\mathrm{clus}}$
Second moment in η in EM2

Cluster depth, $\lambda^{\mathrm{clus}}_{\mathrm{centre}}$
Distance of the shower centre from the calorimeter front face measured along the shower axis

Cluster PS energy fraction, $f^{\mathrm{clus}}_{\mathrm{PS}}$
Fraction of energy in the PS

Cluster core energy fraction, $f^{\mathrm{clus}}_{\mathrm{core}}$
Sum of the highest cell energy in PS, EM1 and EM2 divided by the total energy

Cluster logarithm of energy variance, $\log\langle \rho^2 \rangle^{\mathrm{clus}}$
Logarithm of the second moment in energy density

Cluster EM1 core energy fraction, $f^{\mathrm{clus}}_{\mathrm{core,EM1}}$
Energy in the three innermost EM1 cells divided by the total energy in EM1

Cluster asymmetry with respect to track, $\mathcal{A}^{\mathrm{clus}}_{\mathrm{track}}$
Asymmetry in η–ϕ space of the energy distribution in EM1 with respect to the extrapolated track position

Cluster EM1 cells, $N^{\mathrm{clus}}_{\mathrm{EM1}}$
Number of cells in EM1 with positive energy

Cluster EM2 cells, $N^{\mathrm{clus}}_{\mathrm{EM2}}$
Number of cells in EM2 with positive energy

Tau decay mode reconstruction

π^0 identification score of the first π^0_{cand}, S_1^{BDT}
π^0 identification score of the π^0_{cand} with the highest π^0 identification score

E_{T} fraction of the first π^0_{cand}, $f_{\pi^0,1}$
E_{T} of the π^0_{cand} with the highest π^0 identification score, divided by the E_{T}-sum of all π^0_{cand}'s and $h^{\pm}$'s

Hadron separation, $\Delta R(h^{\pm}, \pi^0)$
ΔR between the $h^{\pm}$ and the π^0_{cand} with the highest π^0 identification score

$h^{\pm}$ distance, $D_{h^{\pm}}$
E_{T}-weighted ΔR between the $h^{\pm}$ and the $\tau_{\text{had-vis}}$ axis, which is calculated by summing the four-vectors of all $h^{\pm}$'s and π^0_{cand}'s

Number of photons, N_{γ}
Total number of photons in the $\tau_{\text{had-vis}}$, as reconstructed in Section 3.3

π^0 identification score of second π^0_{cand}, S_2^{BDT}
π^0 identification score of the π^0_{cand} with the second-highest π^0 identification score

π^0_{cand} E_{T} fraction, f_{π^0}
E_{T}-sum of π^0_{cand}'s, divided by the E_{T}-sum of π^0_{cand}'s and $h^{\pm}$'s

π^0_{cand} mass, m_{π^0}
Invariant mass calculated from the sum of π^0_{cand} four-vectors

Number of π^0_{cand}, N_{π^0}

Standard deviation of the $h^{\pm}$ p_{T}, $\sigma_{E_{\text{T}},h^{\pm}}$
Standard deviation, calculated from the p_{T} values of the $h^{\pm}$'s for $\tau_{\text{had-vis}}$ with three associated tracks

$h^{\pm}$ mass, $m_{h^{\pm}}$
Invariant mass calculated from the sum of $h^{\pm}$ four-vectors

Tau decay mode reconstruction

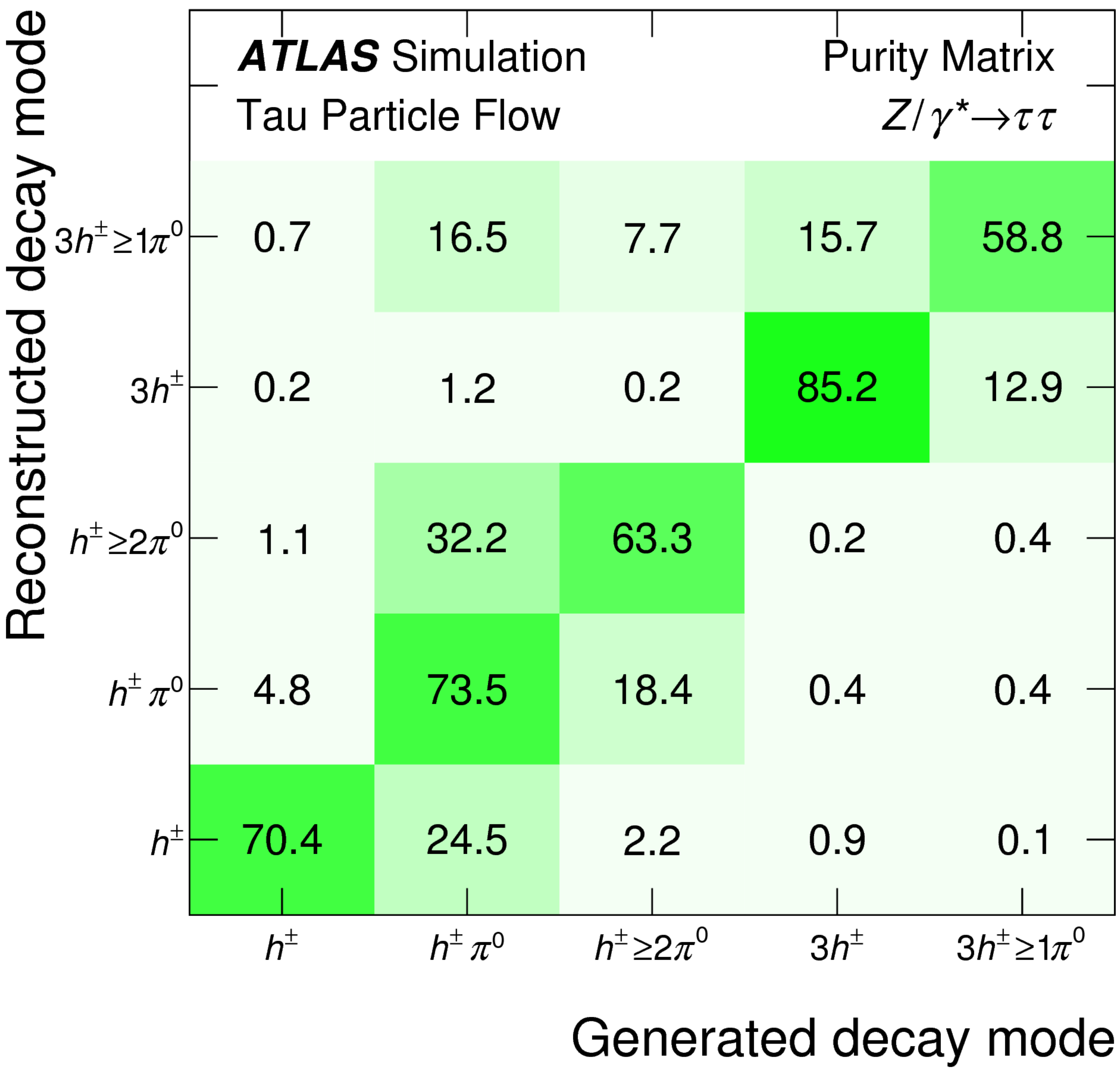

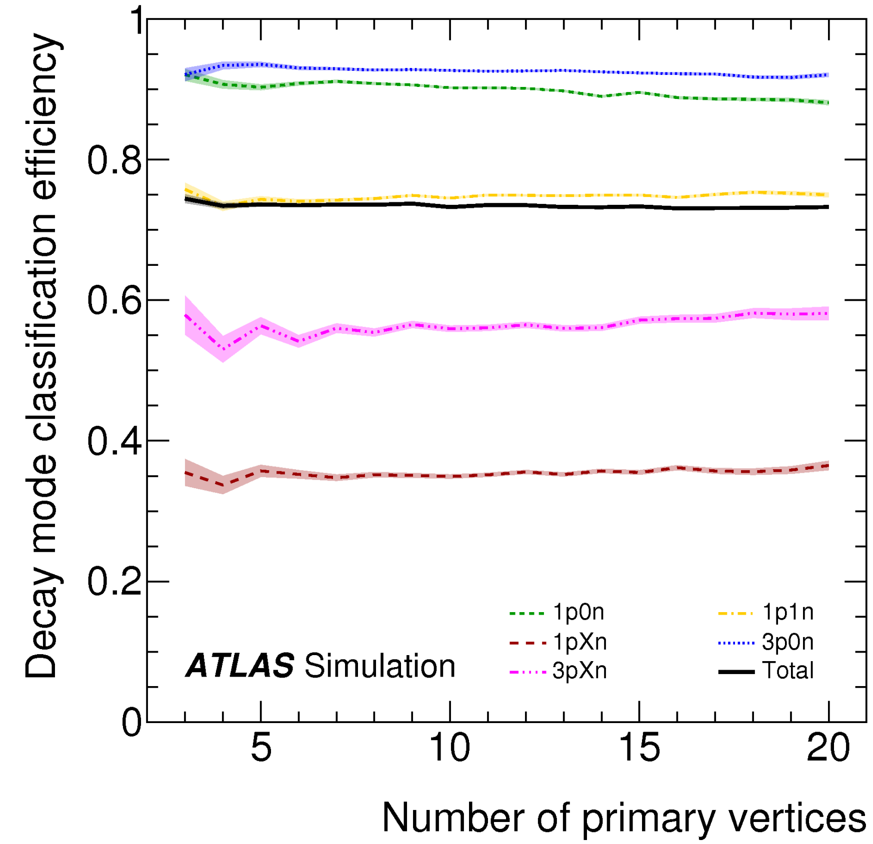

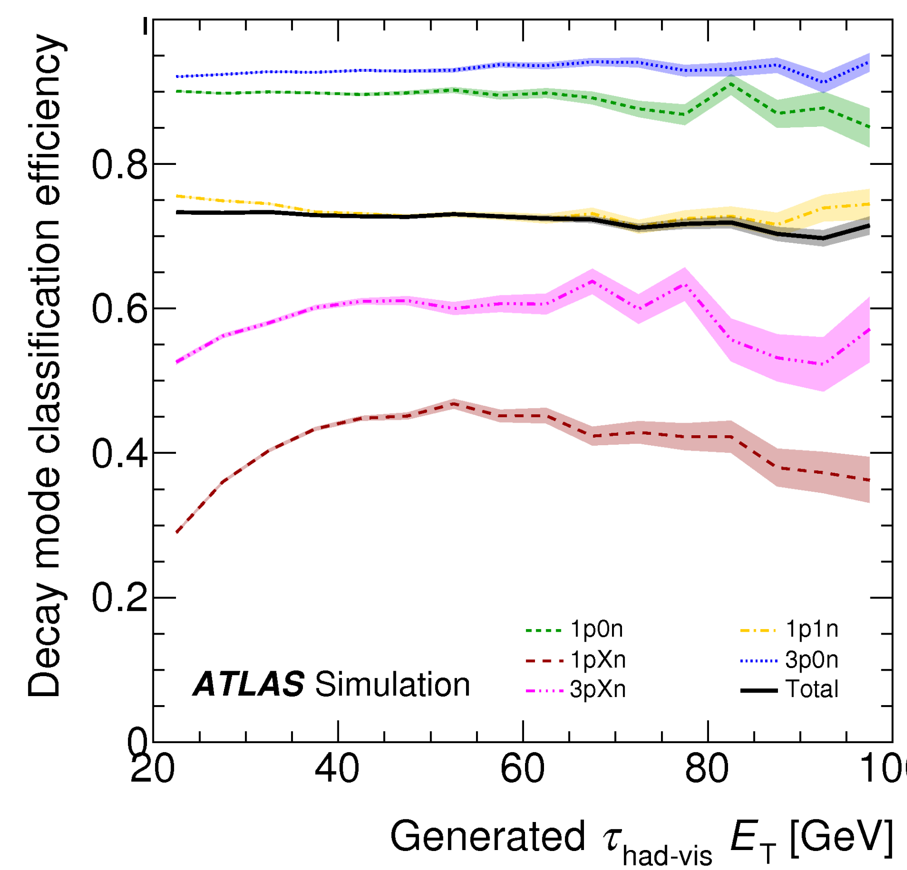

Tau energy BRT

Number of primary vertices, n_{PV}
Number of primary vertices in the event.

Average interactions per crossing, μ
Average number of interactions per bunch crossing.

Cluster shower depth, $\lambda_{\mathrm{centre}}$
Distance of the cluster shower centre from the calorimeter front face measured along the shower axis.

Cluster second moment in λ, $\langle\lambda^2\rangle$
Second moment of the distance of a cell, λ, from the shower centre along the shower axis.

Cluster first moment in energy density, $\langle\rho\rangle$
Cluster first moment in energy density $\rho = E/V$, where E and V represent the energy and volume of the cluster, respectively.

Cluster presampler fraction, $f_{\mathrm{presampler}}$
Fraction of cluster energy deposited in the barrel and endcap presamplers.

Cluster EM-like probability, P_{EM}
Classification probability of the cluster to be EM-like, as described in Ref. [28].

Number of associated tracks, n_{track}
Number of tracks associated with the $\tau_{\mathrm{had-vis}}$.

Number of reconstructed neutral pions, n_{π^0}
Number of reconstructed neutral pions associated with the $\tau_{\mathrm{had-vis}}$.

Relative difference of pion energies, γ_π
Relative difference of the total charged pion energy, E_{charged}, and the total neutral pion energy, E_{neutral}: $\gamma_\pi = (E_{\mathrm{charged}} - E_{\mathrm{neutral}})/(E_{\mathrm{charged}} + E_{\mathrm{neutral}})$.

Calorimeter-based pseudorapidity, η_{calo}
Calorimeter-based (baseline) pseudorapidity.

Interpolated transverse momentum, $p_{\mathrm{T}}^{\mathrm{interp}}$
Transverse momentum interpolated from calorimetric corrections to energy measurement and TPF reconstruction.

Ratio of $p_{\mathrm{T}}^{\mathrm{LC}}$ to $p_{\mathrm{T}}^{\mathrm{interp}}$, $p_{\mathrm{T}}^{\mathrm{LC}}/p_{\mathrm{T}}^{\mathrm{interp}}$
Ratio of the local hadron calibration transverse momentum to $p_{\mathrm{T}}^{\mathrm{interp}}$.

Ratio of $p_{\mathrm{T}}^{\mathrm{TPF}}$ to $p_{\mathrm{T}}^{\mathrm{interp}}$, $p_{\mathrm{T}}^{\mathrm{TPF}}/p_{\mathrm{T}}^{\mathrm{interp}}$
Ratio of the TPF reconstruction transverse momentum, $p_{\mathrm{T}}^{\mathrm{TPF}}$, to $p_{\mathrm{T}}^{\mathrm{interp}}$.